Rijksuniversiteit Groningen

Master Thesis

Star formation suppression, gas consumption and stripping in cluster satellites

Author:
Anatolii I. Zadvornyi

Supervisors:
dr. Kyle A. Oman
prof. dr. Marc A.W. Verheijen

July 1, 2021

Contents

Abstract

Galaxies are affected by their environment, which can shut down their star formation, a process called quenching. Observations show that there is a peak in the quenching timescale of satellite galaxies for satellites of $M_* \approx 10^9\,\mathrm{M}_\odot$; less and more massive satellite galaxies quench on shorter timescales. We investigated the origin of the peak in the quenching timescales as a function of stellar mass using EAGLE cosmological simulations of galaxy formation and evolution. The simulations qualitatively reproduce the observed trend, but place a peak at higher $M_\star$. We select gas particles bound to satellite galaxies at infall time and track their subsequent evolution to find the prevailing mechanism that removes their gas. Low-mass satellites have part of their star forming gas mechanically removed by ram pressure stripping, this effect becomes less effective with increasing stellar mass. Higher mass satellites are quenched relatively quickly by starvation, which becomes less effective at lower masses. Intermediate mass satellites with a characteristic stellar mass of $M_c \approx 10^{9.75}\,\mathrm{M}_\odot$ are at the intersection where both mechanisms are least effective. Galaxies at and below M_c have a virial temperature $\mathrm{T_{vir}}$, low enough such that all of their halo gas can potentially cool on relatively short timescales and fuel the cold reservoir. Galaxies above M_c have high enough $\mathrm{T_{vir}}$ such that the cooling times of fraction of halo gas can be longer that Hubble time: higher mass satellites have to rely on the contents of their cold disc to continue star formation. According to Mitchell *et al.* (2020) $M_* \approx 10^{9.75}\,\mathrm{M}_\odot$ is the mass where the local minimum in outflow rates occurs: at lower mass the outflow rates increase due to supernova winds and at higher mass due to active galactic nuclear winds. A combination of the above mentioned effects makes galaxies at M_c quench on longer timescales. We also find signs of star formation in the ram pressure stripped tails, which is a source of about half of the intra cluster light, with the other half coming from tidally stripped stellar populations. Galaxies that evolve under the influence of a dense cluster environment are affected by a combination of different quenching mechanisms, but the effectiveness of each mechanism depends on host and satellite mass.

Notes form the Author

This work builds on the Author's BSc thesis "Environmental Star Formation Suppression in Galaxy Clusters". That work used the same EAGLE simulation as in this study, but then only "integrated catalogues" were used. These catalogues were produced after the simulation was complete in order to make the simulation outputs more manageable. They contain general galaxy properties such as position, velocity, gas, star and halo mass, star formation rates and others (see section 1.4.3). While using integrated properties allows the work to be done on a regular laptop, some of the (crucial) information is lost. Knowing the individual particle state (being gravitationally bound or unbound to its host galaxy, being star forming or non-star forming) allows for a more in-depth investigation of how galaxy cluster environments affect the evolution of galaxies that have recently became a part of a cluster. In the BSc thesis, the Author independently arrived at similar results found by Wright *et al.* (2019) (see section 4.4) who also used tables of integrated properties of galaxies. They have found that low mass satellites are relatively quickly quenched by ram pressure stripping (strong headwind that a galaxy would feel as it falls through a dense environment), high mass satellites are also relatively quickly quenched by starvation (using all of the star forming gas without replenishing it) and intermediate mass satellites have potentials deep enough to effectively resist ram pressure stripping and sufficiently large cold reservoirs to continue forming stars for longer times. This work is focused on testing this hypothesis for the origin of the peak in the quenching timescale as a function of the stellar mass of satellite galaxies, using all available particle data (section 1.4.1).

1 Introduction

Galaxies are collections of stars, gas and dust which are embedded in dark matter haloes. Galaxies differ by size, colour, morphological type, gas mass fraction, environment and redshift. Many of these properties are correlated with each other. Elliptical galaxies are more massive, redder in colour, gas poor, have ellipsoidal shape and are supported by random motions (Baum 1959). Spirals, on the other hand, are less massive, blue in colour, are gas rich and have a flattened shape due to being rotationally supported. Since these two overarching types of galaxies are so different, there is a reason to believe they have different formation channels. In high density regions, called galaxy clusters, elliptical galaxies by far outnumber spirals (Dressler 1980; Postman and Geller 1984). It is thought that cluster environments, the immediate outer region of the cluster, are responsible for the transformation of spirals in ellipticals after they fall in. The mechanisms that remove the star-forming gas from the infalling spirals depend on the mass of the satellite (internal and external mechanisms are discussed in detail in sections 1.1.3 and 1.3).

1.1 Galaxy formation and evolution

Galaxies form in local overdensities embedded in the large-scale structure of the cosmic web (Baum 1959). The emergence of cosmic structure is currently explained by the inflation theory (Starobinskii 1979). Quantum fluctuations in the vacuum energy, which have driven the exponential expansion of the very early universe, resulted in density perturbations, $\delta\rho/\rho$. These density perturbations attract matter from under-dense regions in a run-away fashion. When the over-density of $\delta\rho/\rho \sim 1$ is reached by the perturbations, they decouple from the cosmic expansion and start to collapse. The content of these perturbations is collisional gas and collisionless dark matter (assuming the cold dark matter model). Dark matter relaxes to an equilibrium without shocks to form a spherical structure. Gas, on the other hand, is heated by shocks to the virial temperature of the halo and reaches hydrostatic equilibrium, it is pressure supported, since cooling in the early universe is very inefficient. Eventually, when the first clouds fragment and collapse, they form the first generation of very massive and short-lived stars. After they end their lives with violent supernova events, they enrich their surroundings with metals, which enables the formation of less massive stars. A gas cycle begins, where the same gas may be reused to form multiple generations of stars as they deposit their gas back into their surroundings.

1.1.1 The cosmic web

Collapsed objects come in a variety of sizes, with the largest of them reaching a mass scale of M^*. Objects with masses $M \gg M^*$ are still growing and collapsing. Objects with $M \ll M^*$ form virialized objects (haloes). Finally, objects of masses $M \sim M^*$ form filaments and walls. The filaments and walls form a complex structure that looks like a web, called "the cosmic web" which is populated by the smaller virialized haloes. Empty space between the filaments are called "voids". Nodes that connect the filaments will become galaxy clusters as the structure continues its gravitational collapse.

1.1.2 Gas cooling and star formation

Eventually, the first generation of extremely massive stars forms. They pollute their surroundings with metals which allows the formation of lower mass stars that live on much longer timescales.

Depending on the gas content and star formation activity, a galaxy is blue or red in colour; some galaxies are gas rich and star-forming (SF) while others are gas poor and have ceased their

star formation for a substantial amount of time. The gas clouds within the galaxies, if sufficiently cold and dense, will become gravitationally unstable and will start to collapse. If the clouds have a way to dissipate the gravitational energy that is converted to heat, then eventually, a (collection) of stars will be formed. Stars, depending on their initial mass, will have different temperatures and lifetimes, with massive ($M_\star \approx 60\,\mathrm{M}_\odot$) stars being white-blue and hot ($T > 30,000\,\mathrm{K}$), remaining on the main sequence for $\sim 10\,\mathrm{Myr}$ and low mass ($M_\star \approx 0.5\,\mathrm{M}_\odot$) stars with lower temperatures ($T \approx 4000\,\mathrm{K}$) that live for a few tens of gigayears. Regions with a high count of young OB stars indicate the presence of large amounts of gas, as they live for a very short time. Conversely, absence of OB stars indicates a lack of star formation activity. Star forming and quiescent galaxies populate two distinct regions on a color-mass diagram. Star forming galaxies are less massive and blue in colour, so they reside in a so-called "blue cloud". Gas poor galaxies with little to no activity, which are typically more massive and redder in colour, reside on a "red sequence". A sparsely populated region in between is called a "green valley" occupied by galaxies that depart from the blue cloud and are on their way to cease star formation, to land on the red sequence.

There are several ways of slowing down or stopping SF; regardless of the cause, if the specific star formation rate, defined as SF per unit stellar mass, $\mathrm{SSFR} = \mathrm{SFR}/\mathrm{M}_\star$, drops below $10^{-11}\,yr^{-1}$, we say that a galaxy is quenched. This limit is the approximate upper boundary of the red sequence in the color-mass diagram. It has been suggested that the main quenching mechanism depends on the mass of the galaxy, ranging from the UV ionisation background for the ultrafaint dwarfs, to ram pressure stripping (RPS) in low mass satellites to starvation in massive satellites.

Galactic gas is cycled between the different *reservoirs*. There are several ways to quench a galaxy, for instance: (i) deplete H_2 and prevent the $\mathrm{H} \rightarrow \mathrm{H}_2$ transition, (ii) remove H^+ and H and deplete the H_2, (iii) deplete the $\mathrm{H} \rightarrow \mathrm{H}_2$ channel and H_2 and prevent the $\mathrm{H}^+ \rightarrow \mathrm{H}$ transition. The multitude of hydrogen gas states depends on its location and its stellar/active galactic nucleus (AGN) activity. A cold disc configuration of gas is a natural thermodynamic outcome of an initially hot sphere of gas that cooled down and retained its angular momentum, while stars can only form in high density regions of the cold disc.

1.1.3 Feedback and mass quenching

Supernova (SN) feedback is thought to be an important mechanism in halting SF in galaxies. SN activity puts an upper limit on the SFR the galaxy can sustain as the lifetime of the most massive stars that end up going supernova is comparable to the proto-stellar core collapse time of ∼10 Myr. The SN feedback by itself may or may not be enough to expel the cold gas from the plane of the disc, but it enhances the effect of other mechanisms, such as RPS and tidal stripping, by pushing the gas out of the plane of the disc and out of the potential well of the galaxy. SN winds play a substantial role in shortening the lifespan of low mass galaxies. Since dwarf galaxies in the local volume within $1 < R/R_{\mathrm{vir}} < 2$ around the Milky Way (MW) and M31 continue their star-formation after infall, SN feedback is expected to keep lifting the cold gas out of the plane of the disc of the satellite, which is then swept away by the denser environment of the Local Group(s), thus depleting cold reservoirs on shorter timescales.

AGN feedback is a self-regulating internal quenching mechanism that injects energy in the form of winds, radiation or radio plasma jets into surrounding gas clouds, preventing them from further collapse and even ejecting them from the galaxy (negative feedback) (Morganti 2017). AGN feedback plays a big role in the evolution of galaxies (both centrals and satellites) with black hole masses $\mathrm{M}_{\mathrm{BH}} > 10^{6.5-7.5}\mathrm{M}_\odot$ (Bluck *et al.* 2020; Correa *et al.* 2019). Star formation is suppressed by AGN feedback in massive galaxies, regardless of them being centrals or satellites

(Donnari *et al.* 2021). Inside-out quenching is a characteristic signature of AGN involvement, as inner regions of the galaxy are affected first. On the other hand, a recent study by Zhuang *et al.* (2021) suggests that AGN activity may exert positive feedback: the star formation efficiency in the inner kpc of the bulge (the innermost spheroidal configuration of "old" stars) and AGN activity are correlated. Similar to RPS, AGN activity can deplete cold reservoirs by ejecting the gas or enhance SFR in its area of effect.

Field galaxies can sustain SF indefinitely, as long as there is a continuous supply of fresh gas from the filaments or walls of the cosmic web. The depletion timescale of the cold gas is shorter than the Hubble time (Oort 1970; Larson *et al.* 1980) suggests that they can only form in the field. As galaxies enter cluster environments, the supply of gas is shut off because the virial temperature of the intra-cluster gas is considerably higher than that of any infalling galaxy, i.e., the intra-cluster medium (ICM) gas is hot enough to move at velocities higher than the escape velocity of any infalling halo. Quenching by using all the available gas for star formation, without replenishing it, is called *starvation* (Brownson *et al.* 2020). High mass satellites $M_\star > 10^{10} M_\odot$ are thought to be quenched relatively quickly by this effect (Wetzel *et al.* 2013; Oman *et al.* 2021), with higher stellar mass satellites depleting their reservoirs quicker, as they have lower gas mass fractions and have higher SFR (van de Voort *et al.* 2017). Furthermore, high mass satellites, before they are quenched, have a stellar mass growth almost identical to centrals, meaning that they do not "feel" the immediate environmental effects (Cochrane and Best 2018).

1.2 Groups and clusters of galaxies

Collections of galaxies that are gravitationally bound are very common. They are called groups, which contain tens of galaxies, such as our Local Group, or clusters, which contain hundreds to thousands of galaxies, such as the Coma cluster. The "host" being the most massive galaxy and "satellites" orbiting it. It is thought that spiral galaxies can only form in the "field" environment, i.e., in a low galaxy density environment as the timescale of disc formation is a few gigayears. This is a typical assembly timescale of a spiral galaxy as the disc structure is very fragile and easily disrupted in a high density environment, or even by a close fly-by of another similar (or more massive galaxy). As galaxies fall into a dense cluster environment, their gas accretion is halted and their existing gas is removed on a similar timescale as it takes a spiral galaxy to form in the field. Furthermore, according to the morphology density relation (Dressler 1980), cluster environments are dominated by elliptical galaxies and the field environments are dominated by spirals. From that, one may infer that cluster environments are responsible for the transformation of spirals to ellipticals. Butcher and Oemler (1984) showed that nearby clusters have spirals that have a redder bulge than the ones in the field indicating that they have started their transformation into ellipticals.

1.3 Environmental quenching

As mentioned before, cluster environments are responsible for halting the accretion of new gas and removing the existing gas in galaxies that fall into them. In this section we discuss the quenching mechanisms that are most relevant to this work and outline other mechanisms that act on the mass scale not covered in this study or were not comprehensively looked into due to their complexity.

1.3.1 Ram pressure

Perhaps the most spectacular quenching mechanism is ram pressure stripping (RPS). As galaxies fall into the cluster environment they feel a "head wind", that is a hydrodynamical pressure that competes against self-gravity of the inter stellar medium (ISM) gas. If RPS is stronger than the restoring force, then the gas will be removed (Gunn and Gott 1972):

$$\rho_{\rm ICM}(r)V^2 > 2\pi G\Sigma_\star\Sigma_{\rm ISM}, \tag{1}$$

where G is the gravitational constant, ρ_{ICM} is the density of the interstellar medium of the satellite, V its relative velocity to the ICM, $\Sigma_\star$ and $\Sigma_{\rm ISM}$ are the surface mass density of the stars in the disc and of the ISM, respectively. Fillingham *et al.* (2015) estimated a critical mass of $M_{star} = 10^8 M_\odot$, below which the self-restoring forces are not strong enough to resist pressures exerted by the ICM onto discs of satellites. The mass of the host system determines the effectiveness of RPS, as more massive clusters will have higher densities. Numerical simulations can give insights into the environmental effects that transform galaxies on gigayear scales. ILLUSTRIS a cosmological hydrodynamical simulation, similar to EAGLE in spatial and mass resolution, used to study formation and evolution of galaxies. Lower mass hosts in ILLUSTRIS simulation have, on average, bluer satellites, suggesting that RPS is less effective (Sales *et al.* 2015) and the density of the cluster affects quenching the most (Bluck *et al.* 2016). Observational studies arrived at the same conclusion (Bluck *et al.* 2020; Mao *et al.* 2021).

RPS can also compress gas in an infalling galaxy that will enhance SF, which depletes their cold reservoirs quicker at the time of the first infall and/or at the pericentric passage (Mistani *et al.* 2016; Wang *et al.* 2020), as at pericentic passage satellites will achieve the highest velocity with respect to ICM and will traverse denser ICM regions of the cluster such that they will feel the strongest winds (Arthur *et al.* 2019). Conversely, satellites with wider orbits, i.e., satellites that traverse the outer, low density regions of the cluster environment at lower orbital speeds will quench slower (Lotz *et al.* 2019). Another study of simulated isolated satellites (Lee *et al.* 2020) suggests that the SFR is enhanced with moderate winds, as they gently compress the cold gas in the satellites (in the cluster outskirts), while strong winds (during pericentric passage) decrease the star formation efficiency by a factor of 2. Either way, cold gas is removed by the means of stripping, or by being consumed in the formation of stars. Furthermore, the effectiveness of RPS depends on the "angle of attack", the angle between the instantaneous velocity vector and the plane of the disc. Face-on infalling galaxies will experience stronger stripping and lower star formation efficiency (SFE) enhancement than the edge-on galaxies, which will feel a considerable enhancement of SFE and weaker stripping (Schulz and Struck 2001; Lee *et al.* 2020). Virgo cluster observations (Morokuma-Matsui *et al.* 2021) suggest that RPS is relevant at $r < 1.5\,R_{vir}$ for the cold gas removal; Bahé *et al.* (2013) demonstrated that RPS can start removing hot halo gas from galaxies already in the filaments that are connected to clusters, at distances up to $\sim 5\,R_{200}$.

1.3.2 Tides

Tidal stripping is a force exerted by a much more massive body (cluster) on a less massive body (satellite), which is stronger on the near side of the less massive body compared to the far side. This results in stretching the lesser body along the line that connects the centre of the potential of the two bodies. Any mass outside the critical radius (tidal radius) of the lesser body will be lost:

$$r_t = \left[\frac{m/M}{3 + m/M}\right]^{1/3} R, \tag{2}$$

where m is a mass of a satellite, M is mass of the point like potential well, and R is the radius of a circular orbit (Mo *et al.* 2010).

1.3.3 Harrassment

Harassment is a cumulative process of high-speed encounters between the members of a cluster that impulsively heat up the gas (increase internal energy) in the galaxies involved (Mo *et al.* 2010). The net result is that the gas in perturbed galaxies is less bound, which enhances other quenching mechanisms, for example RPS and tidal stripping.

1.3.4 Group pre-processing

The same quenching mechanisms that occur in clusters also occur in groups, but their effectiveness is lower (Roberts *et al.* 2021). Galaxies falling in as members of groups are more gas poor, compared to isolated centrals that fall into a cluster directly. This effect is called pre-processing. This mechanism is needed to explain the non-zero fraction of quiescent galaxies in the outskirts of clusters at $4R_{\rm vir}$ (Lemaux *et al.* 2019). At the same time the group environment can act as a shield from RPS when the group falls into a cluster.

Currently, the consensus in the literature is that both direct stripping and halting of the infall of new gas into galaxies are driven simultaneously and may be caused by the same physical processes (Cortese *et al.* 2021). The question is, how deep does ram pressure stripping dig in the cold disc, which then determines how important the consumption of gas by star formation is. Judging from galaxies that survive the first pericentric passage in the Milky Way halo and the Virgo cluster for a few few gigayears, RPS is not very effective at removing star forming gas at low redshift.

1.4 Simulations

Since observations offer only a single (current) stage of the galaxy evolution (or how they looked some time ago, depending on their distance to the observer), one would need a way to observe galaxies from the beginning of times until today. It is done with the help of cosmic simulations, which test current theories and give opportunities to "observe" phenomena that occur on gigayear scales.

1.4.1 The EAGLE simulations

The Virgo consortium's Evolution and Assembly of GaLaxies and their Environments (EAGLE) is a set hydrodynamical simulations The EAGLE team (2017) has developed to study formation and evolution of galaxies on cosmological scales. Gas and dark matter (DM) particles were uniformly distributed in a periodic box and reproduce the matter power spectrum as measured from the cosmic microwave background, giving a set of initial conditions at redshift $z = 20$. The particles were perturbed and were let to evolve untill $z = 0$, where all the cosmic structures have emerged. The simulations solve the Poisson equation for gravity (eqn. 3), the smoothed-particle formulation of the equations of hydrodynamics (eqn. 4 which are thoroughly described by Schaye *et al.* (2015) and Springel (2005)) and subgrid physics (discussed below) which determine the structures that emerge over cosmic time:

$$\nabla^2\phi = -4\pi G\rho \tag{3}$$

and

$$m_i \frac{\mathrm{d}\mathbf{v}_i}{\mathrm{d}t} = -\sum_{j=1}^{N} x_i x_j \left[\frac{P_i}{y_i^2} f_{ij} \nabla_i W_{ij}(h_i) + \frac{P_j}{y_j^2} f_{ji} \nabla_i W_{ji}(h_j) \right] \quad (4)$$

The EAGLE simulations use the following cosmological parameters (Planck Collaboration *et al.* 2014): $\Omega_M = 0.307$, $\Omega_\Lambda = 0.693$, $\Omega_b = 0.04825$, $h = 0.6777$, $\sigma_8 = 0.8288$, $n_s = 0.9611$, $Y = 0.248$. In this analysis only the largest simulation in the suite with $L = 100$ comoving[1] megaparsec (cMpc) was utilised to get the largest possible sample of satellites around clusters and rich groups with masses $M_{\rm host} > 10^{13}\,\mathrm{M}_\odot$. This simulation evolves a collection of 2×1504^3 dark matter (DM) and gas particles of initial mass $1.8 \times 10^6\,\mathrm{M}_\odot$ with maximum gravitational softening length $\epsilon_{prop} = 0.70$ proper[2] kiloparsec (pkpc). The simulation includes processes that act on on scales smaller than the simulation resolution. They are implemented as source and sink terms with a set of differential equations. These "subgrid" processes are designed to be as simple as possible and are set by local hydrodynamical properties (as opposed to pre-determined fixed rules). They include stellar mass loss due to winds from massive and AGB stars, type Ia and II supernovae (Wiersma *et al.* 2009b), radiative cooling and heating of gas (Wiersma *et al.* 2009a), metal-dependent star formation (Schaye and Dalla Vecchia 2008; Schaye 2004), black hole seeding (Springel *et al.* 2005a) and further gas accretion (Rosas-Guevara *et al.* (2015) and as described in Schaye *et al.* (2015)) and AGN heating (as described in Schaye *et al.* (2015)). The old gas phase is not modelled in EAGLE, so a temperature floor of $\mathrm{T} = 8000\,\mathrm{K}$ was implemented. Star formation occurs stochastically and is set by a temperature and density threshold. There are 28 snapshot outputs available between the beginning ($z = 20$) and the end ($z = 0$) of the simulation.

1.4.2 Group finding

Due to finite computing power, to simulate the behaviour of a fluid, the fluid is first discretized on a grid and then all the forces that act on that fluid element are calculated in order to advance the simulation to the next time step. Eventually, the cosmic structure will emerge and evolve according to above mentioned physics. At the final timestep, the universe is at $z = 0$. After the simulation is completed, all particles are grouped using a friend-of-friends group finding algorithm: a particle belongs to a group if it is within linking length l (0.2 $\times$ mean particle separation) to any other member of a group. Every group has a unique identification number. Groups with too few particles are rejected.

To further quantify substructure, a subhalo finder (SUBFIND) algorithm is used, described in detail in Springel *et al.* (2001). In essence, the algorithm begins with estimating the local density field at every position of the DM particle in a given group. Any local overdensity in this field is considered to be a *substructure candidate*, enclosed in an isodensity contour. They are found by gradually lowering the density threshold where the isolated overdense regions will grow in size until they collide with another region at a saddle point in the density field. After all of the substructure candidates are identified, they are checked to be graviationally bound entities. This method is further extended to account for baryonic matter (matter that is made out of at least 3 quarks for example protons and neutrons; and electrons even though they are leptons and not baryons) by assigning a baryonic particle to a neighbouring DM particle, which were assigned in the previous step to be in a sub-structure or not (Dolag *et al.* 2009). Within each identified

[1] Comoving coordinates factor out the expansion of the coordinate system, in this case the expansion of the Universe due to dark energy.

[2] Proper distances do not take expanison of coordinate system into account, expansion of the universe will change proper distance between two points.

group, gravitaionally bound overdensities of particles are considered to be galaxies. The most massive galaxy in a group is assigned a `SubGroupNumber = 0` (`SGN`) and all its satellites are assigned `SubGroupNumber > 0`.

1.4.3 Merger trees

After the simulations were completed the EAGLE team had to, among other things, build merger trees which would allow the linking of galaxies between the snapshots in order to track galaxies through consecutive temporal outputs. They used the D-TREES algorithm (described in detail in Jiang *et al.* (2014)), which uses `ParticleID` to match haloes between snapshots. The galaxy which consists of N particles at snapshot i will have a descendent at snapshot $i + 1$ and the algorithm will identify the descendent that contains the most bound particles from the previous snapshot. A galaxy at snapshot i can only have 1 descendent, however a galaxy at snapshot $i + 1$ can have multiple progenitors. The main progenitor that corresponds to the main branch of the tree is the one which has the largest branch mass, as opposed to just being the most massive progenitor in the tree: that could lead to main branch swapping during similar mass mergers. Since the main progenitor is defined through the largest branch mass, the main branch galaxies can have `SubGroupNumber` $\neq$ `0` (i.e. not a central galaxy in that group). With the above described scheme, any galaxy can be selected and tracked back in time to observe its evolution.

The output data is stored in different databases: there are group catalogues containing lists of objects at each snapshot time, and their integrated properties; there are merger trees which identify objects at a given time with objects at earlier/later times; there are particle snapshots listing particles and their properties at each snapshot time. Each of these data products have indices which allow them to be linked against the others, so the particles of a given object can be identified by their `GroupID`. The object can be tracked through time using the merger trees (required because `GroupIDs` change as objects grow/merge), while the particles can be tracked through time by their `ParticleID`, which is unique.

2 Methods

We extract reference data from the tables of integrated properties of galaxies in order to find which particles belong to a given galaxy at infall time. Different quenching mechanisms have specific footprints on the tracked gas particles, so by tracking the particles that were a part of a galaxy at infall time, we can infer the main physical effect that led to quenching. The following section describes all procedures that took place in extracting and analyzing the particle data.

2.1 Galaxy sample

We selected "host" systems with halo masses $M_{200} > 10^{13}\,\mathrm{M}_\odot$ in the EAGLE RefL0100N1504 simulation at $z = 0$ (snapshot = 28), where M_{200} is the mass that is enclosed by a radius within which the density enclosed is 200 times the critical density of the universe. We then selected the satellite galaxies that are within the infall radius $r_{\rm inf} = 2.5R_{\rm vir}$ of their host galaxy. The radius $2.5R_{\rm vir}$ was chosen as the infall radius because once satellites enter this aperture, most never exit it again (Mamon *et al.* 2004). We use the definition of $R_{\rm vir}$ of Bryan and Norman (1998), as radius of a spherical volume within which the average density is $\Delta_{\rm c}$ times the critical density $\rho_{\rm crit}$:

$$M_{\rm vir} = \frac{4}{3}\pi R_{\rm vir}^3 \Delta_{\rm c} \rho_{\rm crit}, \tag{5}$$

where $\Delta_{\rm c} = 360$. Virial radius $R_{\rm vir}$ is related to R_{200} through $2.5R_{\rm vir} = 3.3R_{200}$. We make this conversion as EAGLE database provides values of R_{200}, R_{500} and R_{2500}. This radius ensures that galaxies are tracked before they enter the cluster environment as gas interaction already begins in outer regions of the cluster and there are no galaxies missed that are turning around during their backsplash. 167 host galaxies in mass range $\log_{10}(M_{200,\rm host}/\mathrm{M}_\odot) = [13, 14.6]$ and 4208 satellites at $\log_{10}(M_\star/\mathrm{M}_\odot) = [9, 11]$ were initially found.

We extracted the merger trees (see Section 1.4.3) for the selected host and satellite systems. These provide a record of the orbital histories of the satellites around their hosts, and the evolution of their properties (such as position, SFR, velocity, group number, subgroup number, snapshot) as a function of time. These tabulated histories are the reference information for extracting particle data presented in next Subsection.

In this work quenching timescale $\tau_{\rm q}$ is defined as time it took for a satellite to quench after it crossed the infall radius $r_{\rm inf} = 2.5R_{\rm vir}$, $\tau_{\rm q} = t_{\rm q} - t_{\rm inf}$, (see Figure 1). Quenching is defined using a definition commonly used in the literature (Baldry *et al.* 2004): satellite's specific star formation rate, $\mathrm{SSFR} = \mathrm{SFR}/\mathrm{M}_{\star,\rm sat}$ dropping below $10^{-11}\,\mathrm{yr}^{-1}$. Typically, quenching corresponds to decrease of SSFR by 2-3 dex. Satellites that quenched before they crossed $r_{\rm inf}$ were removed from the final sample. We note that for all $\tau_{\rm q} - M_\star$ relations (Figures 2 and 3), only the galaxies that have quenched after infall are present, since quenching time is required to calculate the quenching timescales. All other plots are made with the full satellite samples (both quenched and not quenched).

The satellites were chosen to infall between 6-9 gigayears ago ($z \approx 0.6 - 1.5$) in an attempt to have the largest sample with approximately the same properties, since, for example, SFR is redshift dependant and that can affect how a galaxy would interact with its environment.

After examining gas mass histories, we removed galaxies that had more than ~ 5 times the average mass at infall, in order to constrain the sample to consist of more or less similar galaxies. Occasionally, galaxies that were stripped of the majority ($\sim 90\%$) of their stellar mass by $z = 0$, would "wrongly" be associated with lower mass galaxies at infall. These galaxies alone would dominate their respective mass bins (they would have 20 times the average gas mass at infall in their respective mass bin), so they were removed from the final sample.

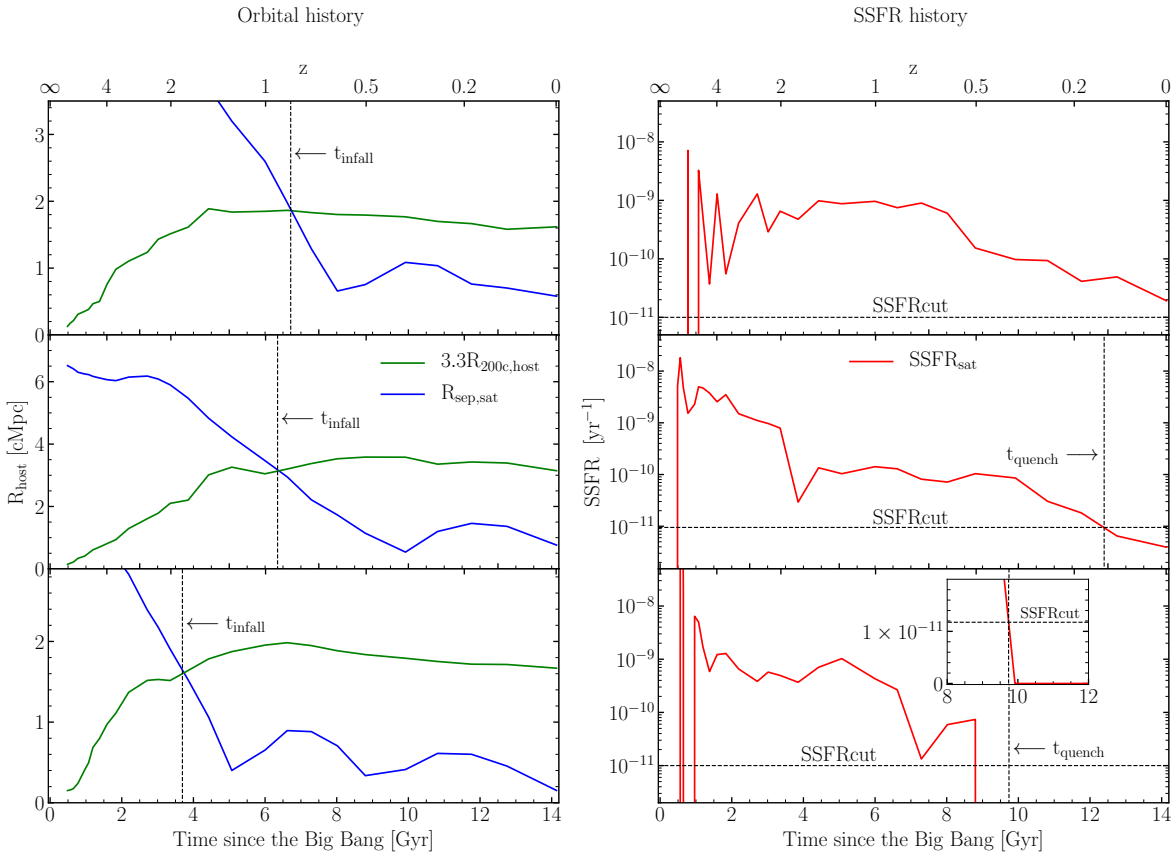

Figure 1: Orbital and star formation histories of 3 example satellite galaxies. *Left*: radial separation between the satellite and the host (blue line) and size of the host, defined as our infall radius of $3.3R_{200}$ (green line). The time when the two curves cross is the infall time $t_{\rm inf}$, marked with a vertical dotted line. *Right*: SSFR as a function of cosmic time of the respective satellites. The time when SSFR drops below SSFRcut $= 10^{-11}\,{\rm yr}^{-1}$, referred to as quenching time $t_{\rm q}$, is marked with a vertical dotted line. For every satellite that quenched after infall we derived quenching timescale $\tau_{\rm q} = t_{\rm q} - t_{\rm inf}$. Top panel shows a SSFR of satellite that was not quenched after infall, middle panel shows a case where a satellite quenched after infall but still has SSFR$> 0\,{\rm yr}^{-1}$ and bottom panel shows a case where SSFR drops to zero after infall (the zoom-in in the bottom right panel shows SSFR on a linear scale).

We also removed galaxies that had a substantial increase (approximately 3 times their current gas mass) in their gas mass after infall, which is a sign of merging since the main focus of this study is to observe how gas is removed and not supplied into satellite galaxies. The final sample consisted of ~ 1500 satellites.

We examined the behaviour of gas in field galaxies and compare them to the gas behaviour in satellite galaxies in order to observe the environmental effects. The partition of initial gas particles into the various baryonic components of central galaxies were stellar mass-matched at satellite accretion. For every satellite in the sample, a field galaxy was matched by mass; stellar mass of field galaxies are within 5% of stellar mass of the respective satellite. We considered only field galaxies that have at most one snapshot with `SGN` $\neq 0$ (are not a central galaxy in their respective group) to ensure that we compare the galaxies that did not experience major mergers and evolved in relative isolation. Furthermore, for each field galaxy, the gas particles were selected at the same snapshot as a respective satellite infall snapshot. Stacked mass evolution plots of lowest and highest baryon partition evolution (section 2.3) of satellites and field galaxies can be seen in Figure 4.

2.2 Particle selection and tracking

Now that we have defined a sample of host systems and their satellites, we move on to tracking their constituent particles through time. By matching the $\mathrm{GN_{sat}}$ and $\mathrm{SGN_{sat}}$ of a given satellite and $\mathrm{GN_{particle}}$ and $\mathrm{SGN_{particle}}$ of individual particles, it is possible to find the particles that belong to a subgroup/galaxy. We recorded gas `ParticleIDs` for every galaxy in our sample at the infall time. This resulted in $\approx 2.2 \times 10^7$ particles for satellites and a similar amount for centrals. A table that contained the evolution history of each particle was then generated in the following way: baryonic matter particles were matched by thier IDs at infall time to particles at later snapshots. The following quantities were tabulated: `AExpMaximumTemperature`, `Coordinates`, `ParticleType`, `Density`, `ElementAbundance`, `GroupNumber`, `InternalEnergy`, `Mass`, `MaximumTemperature`, `Metallicity`, `OnEquationOfState`, `ParticleIDs`, `SmoothedElementAbundance`, `StarFormationRate`, `SubGroupNumber`, `Temperature`, `Velocity`. Full description and details of the above mentioned variables can be found in McAlpine *et al.* (2016).

In order to see how gas particles in different phases behave after infall, all of the gas in each galaxy was separated into initially star-forming and initially non-star forming. Gas particles in EAGLE have a property `StarFormationRate`, which show instantaneous star formation rate of a given particle (The EAGLE team 2017). Since temperature is closely related to SFR, SFR is only non-zero if a particle is cold enough (and is above star forming density threshold). As a shorthand, a gas particle is called "cold" if $\mathrm{SFR} > 0\,\mathrm{M_\odot\,yr^{-1}}$ and "hot" if $\mathrm{SFR} = 0\,\mathrm{M_\odot\,yr^{-1}}$.

We start with a sample of bound particles only, because they define the galaxy at infall time. Then, if they are identified by the group finder as bound to the descendant object of the satellite (known by consulting the merger trees) it is bound, otherwise unbound.

The evolution histories of bound cold and hot gas were obtained by stacking up masses of particles (for each galaxy) which resulted in 6 species: bound and unbound hot gas, bound and unbound cold gas and bound and unbound stars that formed from the gas selected at infall.

2.3 Binning

In order to reveal the trends of particle evolution, we aligned satellite galaxies by infall time and linearly interpolated the sum of the particle masses in each component to a common set of evenly spaced times. These are different to integrated/reduced tables that provide the total information about a given galaxy; if more gas is accreted later, it will not be included in the tracking scheme.

The mass evolution plots are the stacked masses different species in the respective mass bins. The satellites were ranked by stellar mass at $z = 0$ and split into 6 bins with equal counts (the influence of this binning choice is discussed in Section 4.1). Furthermore, each mass bin was split into lower 35% and upper 35% by different properties, for example by gas mass fraction at infall, by the impact parameter b/R_{200} of the orbit of the satellite around the host, measured at the time the satellite crosses R_{200} of the host by quenching time scale, the radius that encloses half of their stellar mass $R_{\mathrm{half},\star}$ (i.e. their size). Each property splitting shows different trends on gas contents and how it changes over time for different mass bins. This is discussed in detail in Section 3.

3 Results

In the following section we discuss the measurements of quenching timescales, mass partition between the baryonic phases as a function of time of centrals and satellites, and the source of intra-cluster light. In all of the above mentioned works the mass of the host system differs considerably, which requires the interpretation to be in terms of general trends and not in quantitative terms.

3.1 Quenching timescale

We begin by assessing whether the EAGLE simulations reproduce the trend in quenching timescale as a function of stellar mass implied by observations (Fillingham *et al.* 2015) and another cosmological hydrodynamical simulation ILLUSTRIS (Mistani *et al.* 2016). As mentioned earlier, we select a sample of host galaxies of masses $\log_{10}(M_{200}/\mathrm{M}_\odot) = [13, 14.6]$, then we select satellite galaxies that are within $3.3_{200,\mathrm{host}}$ of their respective host and track them back in time to find when they crossed $2.5R_{\mathrm{vir,host}}$. We then start our "stop watch" and track every satellite galaxy until their quenching time t_q, the point when SSFR $< 10^{-11}\,\mathrm{yr}^{-1}$. The difference between the quenching time and the infall time is called the quenching timescale, $\tau_\mathrm{q} = t_\mathrm{q} - t_\mathrm{inf}$. We compare quenching timescales as a function of stellar mass of EAGLE satellites and observational measurements of Fillingham *et al.* (2015) (F15 hereafter) in Figure 2. For EAGLE satellites vertical bars show the interquartile width of the distribution, not an uncertainty. Qualitatively, the same trend is recovered: more and less massive satellites quench more quickly than intermediate mass satellites. The turnover point is at a different characteristic stellar mass $\mathrm{M_c}$: observations suggest that $M_c = 10^9\mathrm{M}_\odot$ while in EAGLE $M_c = 10^{10}\mathrm{M}_\odot$. Note that the different measurements plotted use different definitions for the quenching timescale. F15 used virial radius of the Milky Way (MW) to set the infall time. Wheeler *et al.* (2014) took the infall time of dwarf galaxies to their groups, that later fell into the MW-like galaxies and not the infall time to MW-like haloes directly. Wetzel *et al.* (2013) (W13 hereafter) used time of first infall to its parent group, similar to Wheeler *et al.* (2014). In this work we used $2.5R_{\mathrm{vir,host}} = 3.3R_{200,\mathrm{host}}$ as the infall radius, without distinguishing the infalling galaxies being isolated or a part of a group. In all cases the quenching time was recorded when SSFR $< 10^{-11}\,\mathrm{yr}^{-1}$.

The results of Mistani *et al.* (2016) very closely resemble the findings of this work. The quenching timescales of ILLUSTRIS satellites follow the same trend and are in a good agreement with τ_q of EAGLE satellteis. Their peak in quenching timescales is at $\mathrm{M}_\star \approx 8 \times 10^9\mathrm{M}_\odot$ around host systems of $\log_{10}(M_{200}/\mathrm{M}_\odot) = [13.8, 14.8]$. Their infall radius was set to the point when the satellite reached its maximum mass. Our definition of infall at $3.3R_{200}$ is very similar as EAGLE satellites just start losing some mass at this distance to the cluster. The current two simulations appear to be consistent with each other with regard to quenching mechanisms but do not reproduce the quantitative observational results.

To investigate which internal mechanisms have the largest impact on the τ_q, we separated the sample by its internal properties. Separation in the total gas mass at infall and the radius that encloses half of stellar mass $R_{\mathrm{half},\star}$ at $z = 0$ can be seen in Figure 3. Splitting galaxies by gas mass (lower and upper 35% of the population in the respective mass bins) separates the populations that quench more quickly from those which quenches more slowly. Both of the subsamples preserve the earlier trend of intermediate mass satellites still taking longer to quench, albeit the peak for the gas rich satellites moves to the lower mass bin at $M_* \approx 10^{9.6}\,\mathrm{M}_\odot$.

Separating the galaxies by radius that encloses half of stellar mass $\mathrm{R_{half,*}}$ at $\mathrm{z} = 0$ brings up another trend: low mass compact satellites (the most compact 35% of the population) tend to have longer quenching timescales than their diffuse counterparts (the most diffuse 35% of the

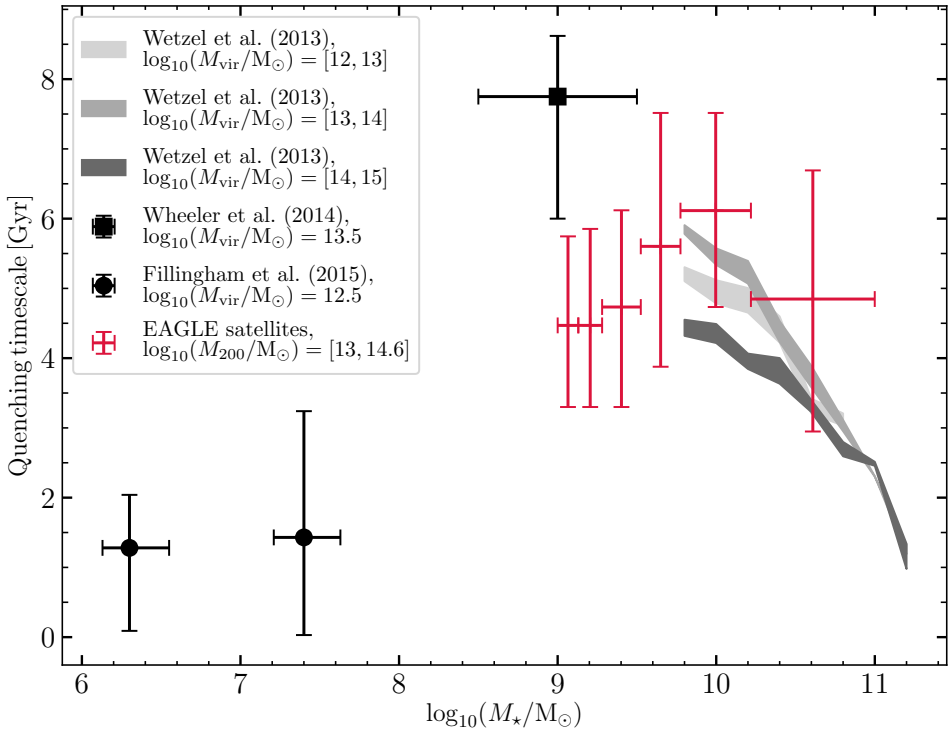

Figure 2: Quenching timescale as a function of satellite stellar mass. Data points in grey and black show observational results obtained by F15 (black points), W13 (shaded bands) and Wheeler *et al.* (2014) (black suqare). Red crosses show bins widths and interquartile width of the distribution of quenching timescales of EAGLE satellites in the respective mass bins. At the higher mass end $M_* \approx 10^{10-11}\,{\rm M}_\odot$ observations show that satellites have decreasing quenching timescale with increasing stellar mass; at the low mass end, $M_\star \approx 10^{6-8}{\rm M}_\odot$ satellites also have relatively short quenching timescale at $\tau_{\rm q} \approx 1.5\,{\rm Gyr}$; intermediate mass satellites $M_\star \approx 10^9\,{\rm M}_\odot$ have the longest quenching timescales at $\tau_{\rm q} \approx 8\,{\rm Gyr}$. This suggests that lower and higher mass satellites are affected by different quenching mechanisms. EAGLE satellites show a similar trend of intermediate mass satellites having longer quenching timescales than lower and higher mass satellites, however the peak is at $M_* \approx 10^{10}{\rm M}_\odot$. While the simulations do not appear to reproduce the measurements in quantitative detail, they do capture the qualitative trend of a peak in the quenching timescale at intermediate satellite stellar mass.

population). This can be explained by deeper potential wells in compact satellites that can better resist RPS, compared to shallower wells in the diffuse satellites. This is the only parameter that causes the quenching timescales of the separated subsamples to cross at the intermediate mass, as on the higher mass end the situation is flipped: diffuse satellites take longer to quench than their more compact counterparts. More compact systems can sustain somewhat higher SFR due to their deeper potential wells keeping their gas at higher densities, which, in turn, increases their SFR and hence they deplete their cold reservoirs more quickly.

3.2 Baryoinic mass partition

3.2.1 Centrals

In order to disentangle internal and external effects that expel or remove gas particles from satellite galaxies, we examine the behaviour of field galaxies first to provide a reference measurement. The top panels of Figure 4 show the stacked mass evolution of the central galaxies in the least and most massive mass bins. We note that there is continuous inflow of fresh gas from the filaments after the point at which we started tracking the respective sets of particles (bottom panels of top figures). This exercise was performed to see how much gas is expelled via internal feedback. In total there are 6 species of particles: bound and unbound particles (darker and lighter colours respectively), non-star forming and star forming gas and stars (red, blue and green respectively). For brevity, non-star forming (nSF) and star forming (SF) gas are interchangeably referred to as "hot" and "cold" gas respectively, as being nSF and SF is closely related to the temperature of the gas.

The top panel in the top left plot in Figure 4 shows the stacked evolution (made by averaging the particle masses from all galaxies in a given bin in stellar mass) of initially cold gas of central galaxies of the lowest mass bin. Some of the initially cold gas will eventually transform into stars, some of the gas will be heated and some of the gas will be heated and expelled by some internal mechanism(s).

The second panel of the same plot shows the evolution of initially hot gas. Some of this gas will be expelled by some internal mechanism(s), some of it will cool down and a subset of the cooled gas will form stars. The third panel shows a combined view of the initially cold and hot gas. The forth panel shows a continuous accretion of gas that is not part of the tracked gas. The black line shows the total bound gas mass, while the magenta line shows the mass of the initially selected gas that is still bound to the galaxy.

The top right panel of Figure 4 shows a mass evolution of the highest mass bin galaxies. The top right plot in Figure 4 is broadly similar to the top left plot, but upon closer inspection one can observe that in the top panel (initially cold gas) the fraction of stars that were produced from the initially cold gas is higher. About 50% of the initially cold gas is transformed into stars in the highest mass bin, compared to 30% in the lowest mass bin. Furthermore, the galaxies in the highest mass bin produce half of the final stellar mass in the first $\sim 0.8\,\mathrm{Gyr}$, while galaxies in the lowest mass bin produce half of the final star mass in about $\sim 1.2\,\mathrm{Gyr}$. This is consistent with observational results of higher mass galaxies having higher star formation rates, as these galaxies have a larger $\mathrm{SFR}/M_{\mathrm{gas}}$ (inverse of depletion timescale τ_{depl}), compared to galaxies in lower mass bins. This is also the first hint for starvation being the main quenching mechanism in higher mass satellites, as a larger fraction of cold gas is consumed through star formation, compared to lower mass bins, in which a lower amount of gas is consumed through star formation and some is "consumed" via RPS, which is discussed in detail in Section 3.3.

The top panels lack unbound cold gas which indicates that the gas that was expelled was heated up before being ejected. This points to SN and AGN feedback. It is not the case for

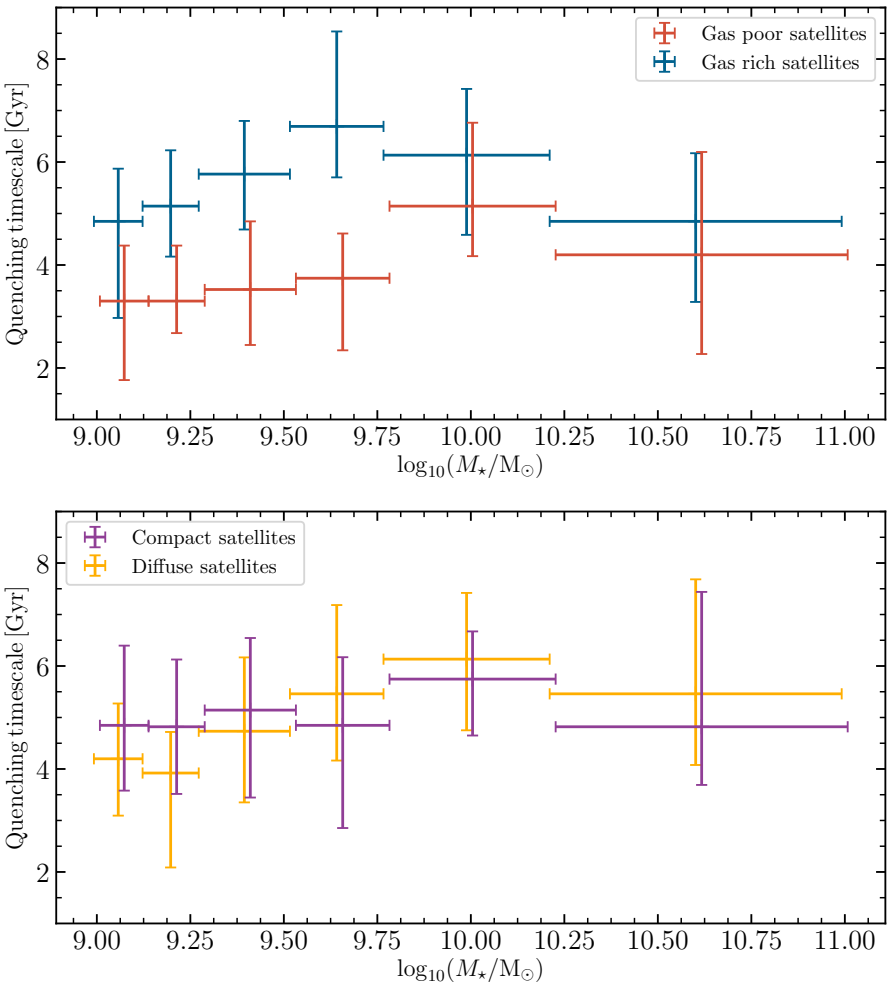

Figure 3: *Top panel* shows quenching timescale as a function of stellar mass of EAGLE satellites split by gas mass fraction. The mass bins are represented by the width of the cross and the height shows the interquartile range. Red crosses show the lower 35% of the population in each mass bin, i.e. gas poor satellites; blue crosses show the upper 35% of the population, i.e., gas rich satellites. The trend of intermediate mass satellites having longer quenching timescales is preserved, however the peak has moved to $M_\star \approx 10^{9.6}\,\mathrm{M}_\odot$ for the gas rich satellites. Gas rich and gas poor satellites have approximately the same amount of cold gas but gas rich satellites have approximately 5 times as much hot gas compared to gas poor satellites. *Bottom panel* shows quenching timescale as a function of stellar mass of EAGLE satellites split by radius that encloses half of the stellar mass $\mathrm{R}_{*,\mathrm{half}}$. Yellow crosses show the lower 35% of the population in each mass bin, i.e. compact satellites; violet crosses show the upper 35% of the population i.e. diffuse satellites. On the low mass end, the diffuse satellites tend to quench more quickly than the compact satellites; on the high mass end, the more compact satellites are quenched quicker than the diffuse counterparts.

the largest mass bin, as there is a trace amount of unbound cold gas: in EAGLE simulations AGN feedback can blow up "bubbles" of hot gas that can push out cold gas without heating it. It may also be due to more massive galaxies being metal rich, hence the expelled gas can cool efficiently and hence there is a trace amount of unbound cold gas and stars that form from the cold unbound gas.

3.2.2 Satellites

Now that the baseline evolution for galaxies not subject to the physics affecting satellite galaxies has been established, we continue by examining the environmental effects that shape out the satellites. Bottom left plots of Figure 4 show mass partition between baryonic matter phases as a function of time of satellite galaxies in the lower mass bin. The top panel shows the evolution of initially cold gas. As in low mass centrals case, some of the gas will heat up, large fraction of which will be expelled, and some of it will turn to stars. Satellites, however, have a non-negligible amount of cold gravitationally unbound gas and stars (from now on, "unbound" referrers to "gravitationally unbound" state of any mass species). Cold gas being stripped without heating is the direct consequence of ram pressure stripping. Low mass satellites produce a lower fractional amount of stars from the initially cold gas, slightly more than 20%. Furthermore, star formation continues in the cold tails and some of the stars are tidally stripped during the host-satellite interaction. This results in about a third of total stars produced from the initially cold gas to be unbound after 6 gigayears of orbital evolution.

The second panel of the bottom left plot shows the mass evolution of initially hot gas of low mass satellites. Compared to low mass centrals, low mass satellites have a substantial fraction of unbound cold gas which cooled down and that was stripped by ram-pressure winds. Likewise, there are unbound stars that were formed in tails and those which were stripped by tides since star particles are not affected by ram pressure. The third panel shows a combined view of initially cold and hot gas.

The fourth panel shows the total tracked bound mass and total bound mass of low mass satellites. As accretion of new gas in cluster environments is forbidden by virial temperature arguments, minor mergers may still bring new gas. Total bound gas and total tracked bound gas do not match perfectly, but they both decrease monotonically, in contrast with centrals, which have a constant inflow of fresh gas.

The bottom panel shows a normalized distribution of quenching times since infall. Some of the quenching times may be longer than 6 gigayears because of the selection effect. Some galaxies have fallen in 5 Gyr after the Big Bang and some fell in after 8 gigayears, so the galaxies that fell in earlier, had 3 more gigayears to interact with ICM, which may have resulted in quenching timescales longer than 6 gigayears. The median of these quenching timescales can be seen in Figure 2, the left most red cross.

The bottom right plots of Figure 4 show the mass evolution of the most massive satellites. The top plot shows the mass evolution of initially cold gas. Remarkably, the shape of the green "wedge" (stars produced out of initially cold gas) has a very similar shape to a wedge of high mass central galaxies (top panel of top right plot of Figure 4). This suggests that massive satellites continue their star production in a very similar manner to massive centrals and there is minimal effect of the ICM environment. There is still a trace amount of cold unbound gas and stars, which points to weak RPS. The second panels show the mass evolution of initially hot gas and the third panels show a combined view of initially cold and hot gas. The fourth panels show total bound tracked mass and total bound gas. A rather notable difference in mass is due to minor mergers that bring a considerable amount of gas to the infalling sytems, as massive satellites will have their own smaller satellites. The bottom panels show normalised quenching timescale

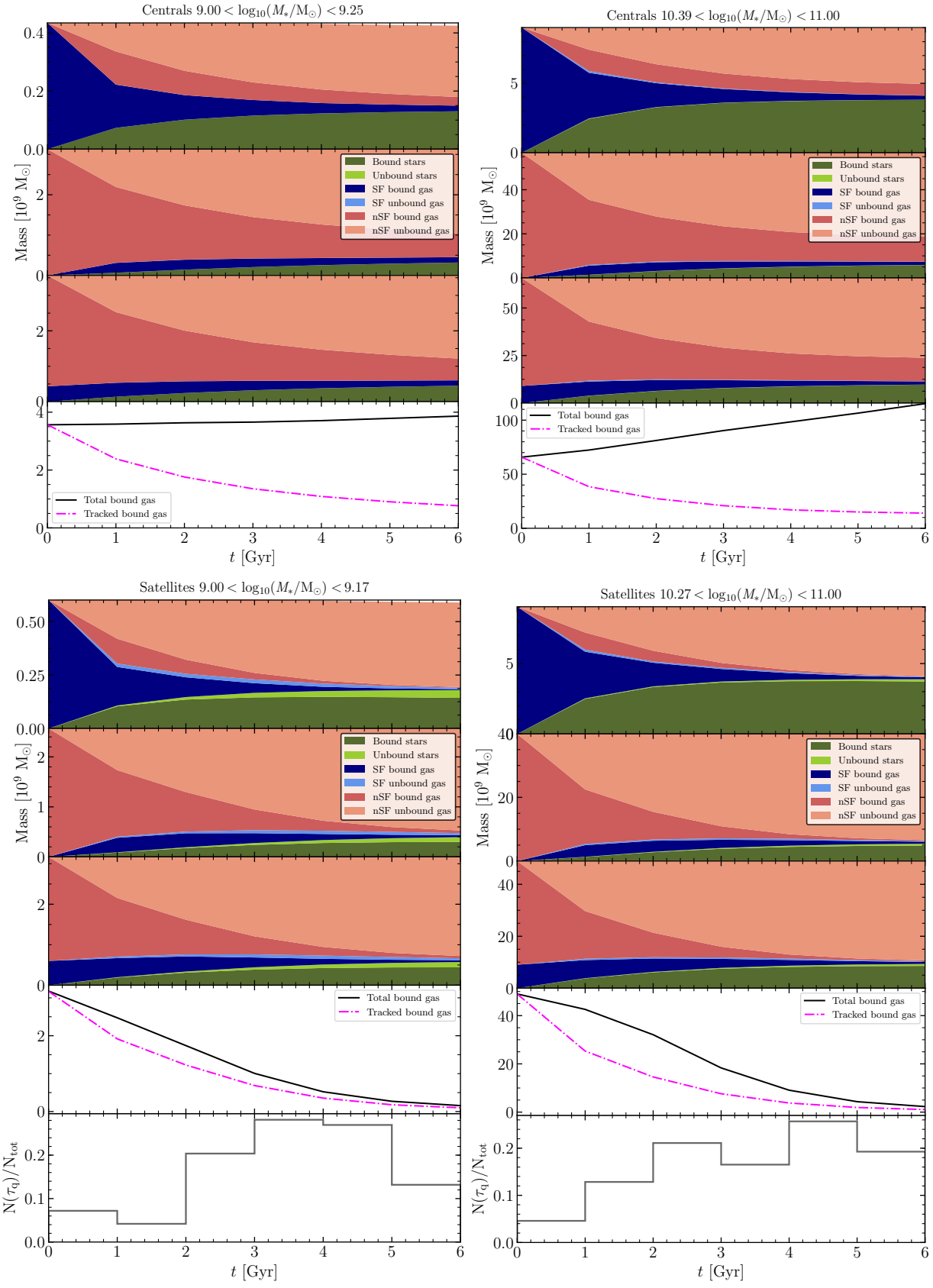

Figure 4: Mass partition between baryonic matter phases as a function of time of central and satellite galaxies in most massive and least massive mass bins. *(continued on next page)*

Figure 4: *(continued) Upper left* Low mass central galaxies. The first panel shows the evolution of the initially cold gas. Blue (light blue) represents star forming bound (star forming unbound) gas mass, orange (salmon) represents non-star forming bound (non-star forming unbound) gas mass and green (light green) represents bound star (unbound star) mass. The second panel is similar, but for the initially non-star forming gas. The third panel is also similar but for both star-forming and non-star forming gas. The last panel shows total bound gas mass and tracked bound gas mass of galaxies. *Upper right* Similar to upper left, but for massive central galaxies. *Lower left* Similar to upper left but for low mass satellites. The fifth panel show the normalised counts of quenching timescales. Notice a non-zero amount of unbound non-star forming gas against no unbound non-star forming gas in least massive centrals. Furthermore, notice that all gas is removed in satellites after 5-6 gigayears. *Lower right* is similar to lower left but for massive satellites.

distribution, its median is plotted in Figure 2.

Satellite galaxies consume or lose all of its initially bound gas at 6 gigayears for the lowest mass bin and after 5 gigayears in the highest mass bin, which is not the case for centrals. There are also very noticeable differences in mass evolution of low mass and high mass satellites. As star formation rates of galaxies are tightly correlated to their stellar masses (Elbaz *et al.* 2007), there are almost 2 orders of magnitude difference in the star formation rate of $M \approx 10^9\,\mathrm{M}_\odot$ and $M \approx 10^{11}\,\mathrm{M}_\odot$ galaxies. Hence the more massive galaxies consume more gas via star formation in a fixed amount of time, as compared to low mass galaxies. This can be observed in the top panels of the bottom plots in Figure 4. In 3 gigayears, almost all of the gas that will be turned to stars is converted: in low mass satellites this is only about a quarter of the initially star-forming gas, whereas in the most massive satellites about a half of the initially star-forming gas will be converted to stars. This already hints that high and low mass satellites have different main modes of gas removal.

A notable difference between the field galaxies and satellites (bottom panels of Figure 4) is that the field galaxies eject a considerable fraction of hot gas (top 3 panels) after 6 Gyrs. This means that there is a rather aggressive feedback and star formation cannot consume all the tracked gas.

3.2.3 Satellite populations split by internal properties

Satellite galaxies split by **total gas mass** (lower and upper 35% of the population) can be seen in Figures 5 and 6. The largest difference in gas mass lies in the size of the hot halo (second panels). Cold discs (top panels) are about twice as massive but haloes are about 6.5 times as massive in gas-rich satellites, compared to gas poor satellites in the low mass bin (Figure 5) and 5 times as massive in the most massive satellites (Figure 6). The cold disc is more prone to RPS in gas poor satellites than in gas rich ones. Presumably, the coronal gas acts as a shield and since gas rich satellites have bigger/thicker "shields" they are more resistant to stripping. Therefore, the hot halo is depleted faster in gas poor satellites and hence the access to the large reservoirs is denied at an earlier time, resulting in the shorter quenching timescale.

The most massive, gas rich satellites survive for longer simply by virtue of having more gas at infall: it takes a longer time to deplete a larger reservoir than a smaller one at a fixed star formation rate.

Galaxies split by **radius that encloses a half of stellar mass** $R_{\mathrm{half},\star}$ are shown in Figures 7 and 8. Most noticeable differences in their gas consumption/stripping can be seen in second

panels (initially hot gas) of masses $M_\star \approx 10^{9.1}\,\mathrm{M}_\odot$. Diffuse satellites tend to lose more of their initially hot gas that cooled down. This may be due to supernova winds that can more easily blow the gas out of shallower potential wells. Contrastingly, the compact satellites can resist the blow out due to their deeper potential wells. Since the hot halo gas is a substantial gas reservoir which can cool down and precipitate back onto the disc, more diffuse satellites are quenched more quickly. They blow out a larger fraction of their coronal gas and they are more susceptible to RPS. More compact satellites can more effectively resist both the SN feedback and RPS.

In the most massive mass bin (top panels) in compact satellites the cold reservoir is depleted after 2-3 Gyrs, whereas in diffuse satellites it is depleted after 4-5 Gyrs. As mentioned before, this is due to the ability of compact satellites to keep the gas at higher pressure so that higher SFR is sustained. Examining the initially hot gas (second panels), one can observe that the hot gas is also depleted faster: strong supernova winds from the intense star formation push out coronal gas that is swept away by ram-pressure winds. Again, the hot halo reservoir is removed faster, which denies access to the gas that can potentially cool down sufficiently and become star-forming (see Section 3.4).

Splitting the galaxy population by **impact parameter**, b shows yet another trend (Figures 9 and 10). Low mass galaxies with tight orbits (left plot, top panel) have a substationally larger amount of cold gas removed without heating, as compared to high b satellites (right plot, top panel) and they have about a third of the stars formed end up in other systems, compared to $\sim 1/6$ in satellites with wide orbits. This is due to the ram pressure being proportional to v^2, tighter orbits will have higher velocities; to ρ_{env} which increases towards the centre of the host system and galaxies with low impact parameter will traverse those regions; satellites that fall through the inner regions of the cluster will be tidally stripped, hence a fraction of star particles end up being gravitationally unbound. Low mass satellites seem to be affected by RPS more than the high mass satellites: they have a substantial amount of cold unbound gas and unbound stars, compared to high mass satellites. Furthermore, there is no substantial difference between the low b and high b at high mass end, suggesting that RPS does not play a significant role in quenching of the high mass satellites.

3.3 Star formation efficiency

We attempt to summarise several of the above trends (Sections 1.3 and 3.2) and quantify how environmental effects affect the star formation rates of satellite galaxies. We estimate star formation efficiencies (SFEs) for galaxies in our sample as $\varepsilon_\star = \Delta M_\star / M_{\mathrm{gas,c}}$, where $\Delta M_\star$ is the mass of the stars that formed from the cold gas selected at infall and $M_{\mathrm{gas,c}}$ is the cold gas mass at infall.

Figure 11 shows the SFE of centrals and satellites normalized by SFE of centrals in respective mass bins. Vertical bars show the interquartile range. The discrepancy of 20% at the low mass end between the centrals and satellites suggests that there is an environmental effect (presumably RPS), which disrupts the cold disc. This effect is less effective with increasing stellar mass – there is only 6% difference the centrals and satellites in the highest mass bin. This shows that RPS is most effective at lower masses, where self-gravity of the gas in the satellites is not strong enough to resist the ram-pressure wind.

Figure 11 is the closest we have been able to come to a summary plot that would encompass all trends discussed earlier. This, however, is not the full picture. The current description does not take into account the whole gas cycle (heating and cooling) and it ignores the contribution of the initially hot gas to the final stellar mass fraction. There were attempts at constructing a simple model that would predict how much stellar mass a central galaxy would produce, given its initial conditions (hot and cold gas mass and their SFR) in order to apply it to satellites

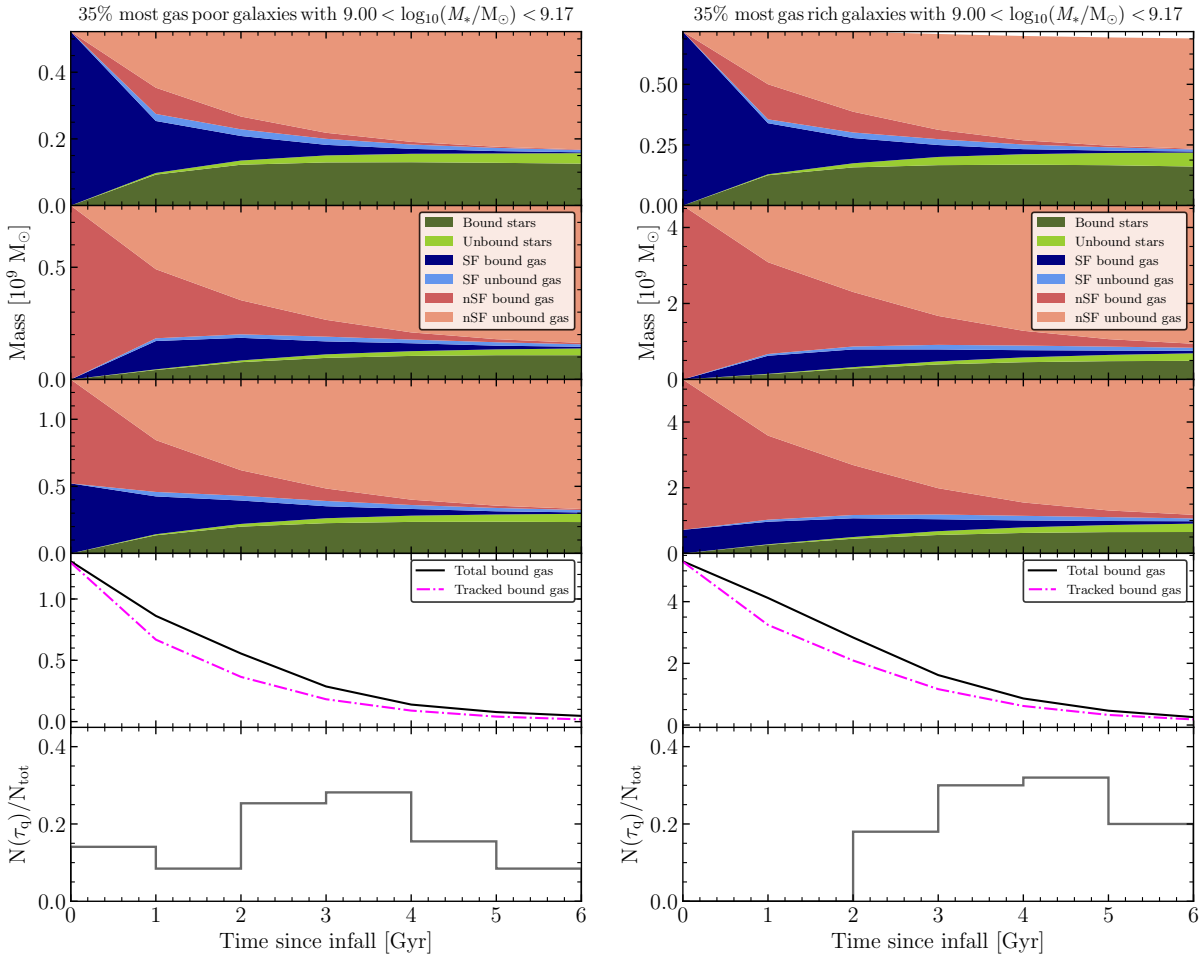

Figure 5: Similar to Figure 4 but for satellite galaxies in the least massive mass bin, *split by gas mass at infall*. The colour coding of different mass species is the same as in Figure 4.

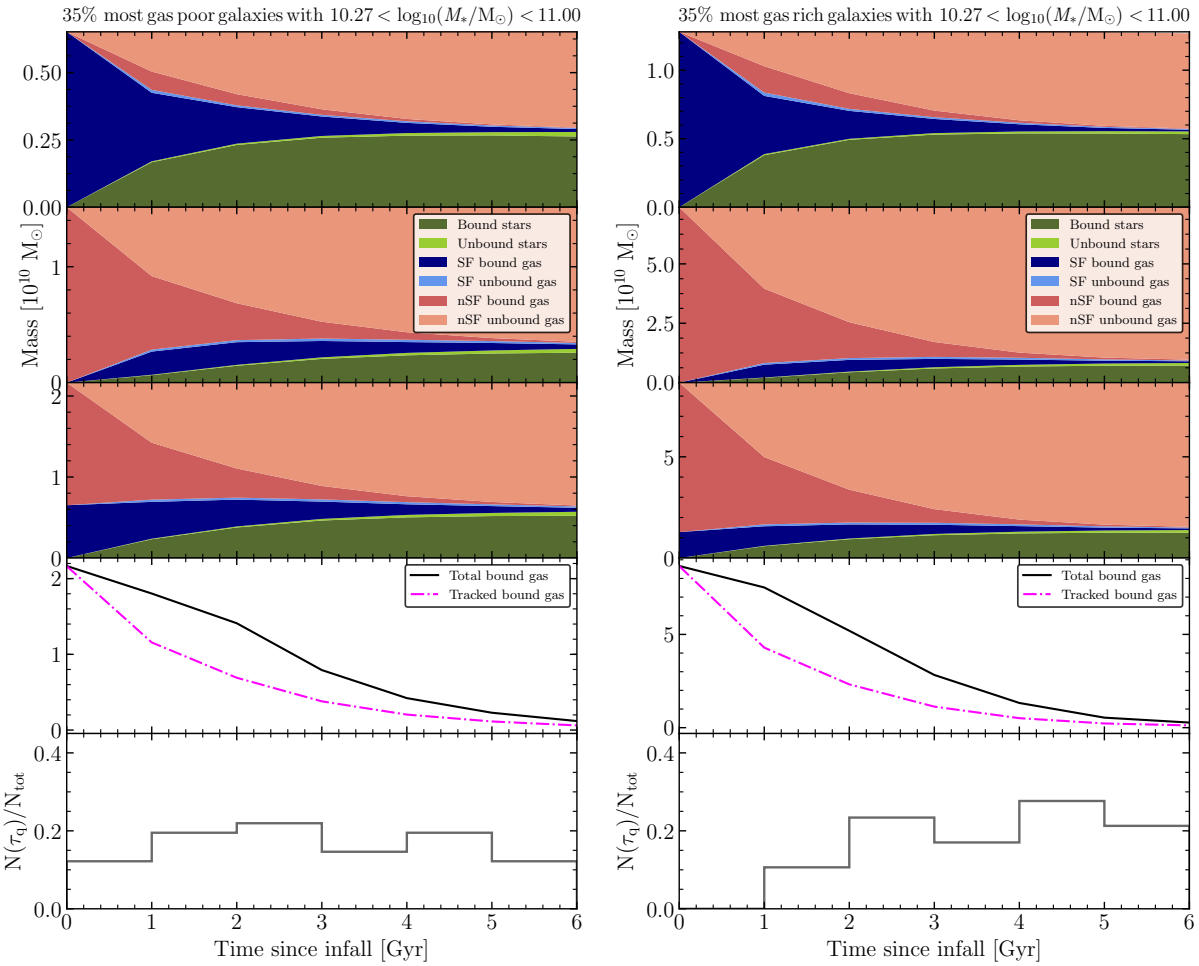

Figure 6: Similar to Figure 4 but for satellite galaxies in the most massive mass bin, *split by gas mass at infall*. The colour coding of different mass species is the same as in Figure 4.

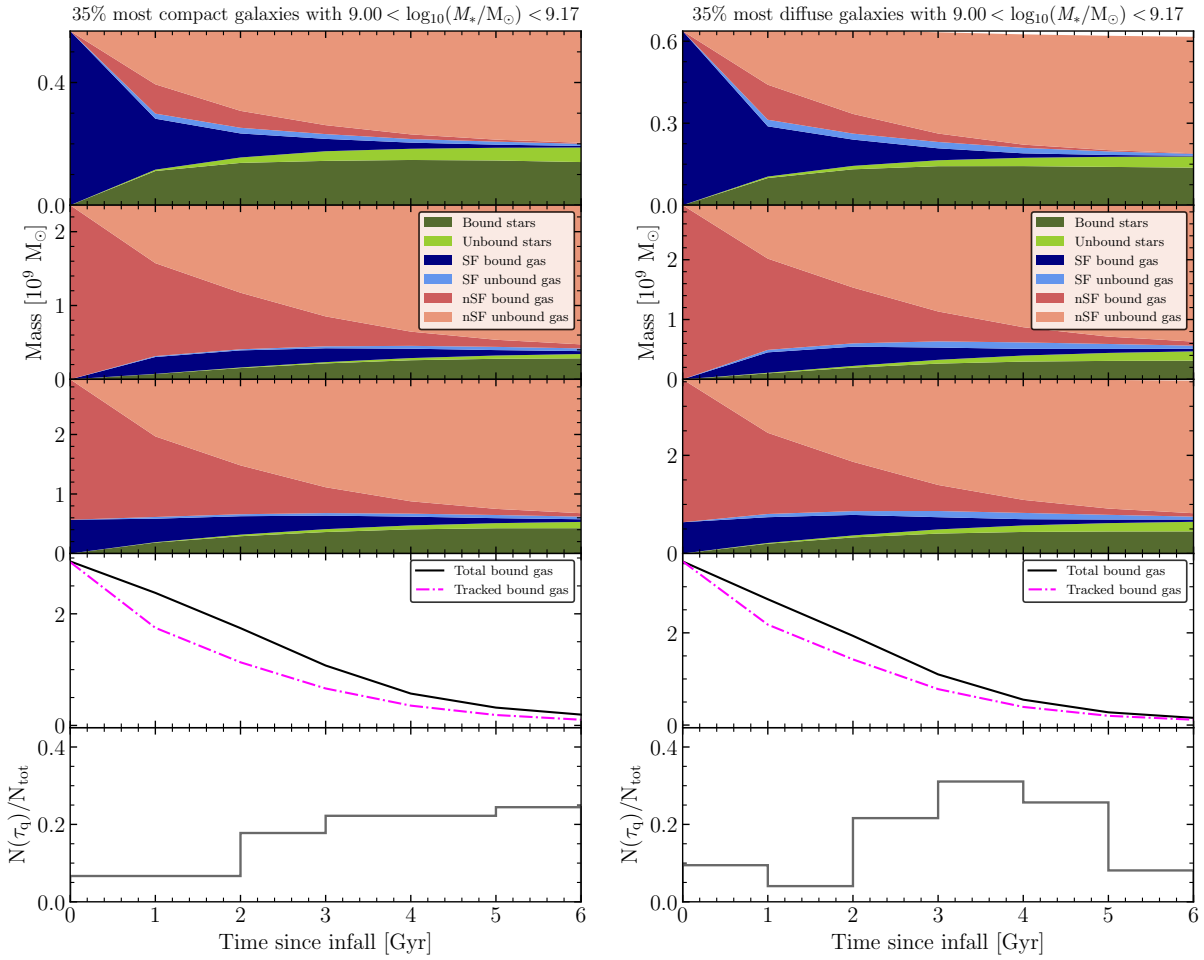

Figure 7: Similar to Figure 4 but for satellite galaxies in the least massive mass bin, *split by* $R_{\star,\mathrm{half}}$ *at* $z = 0$. The colour coding of different mass species is the same as in Figure 4.

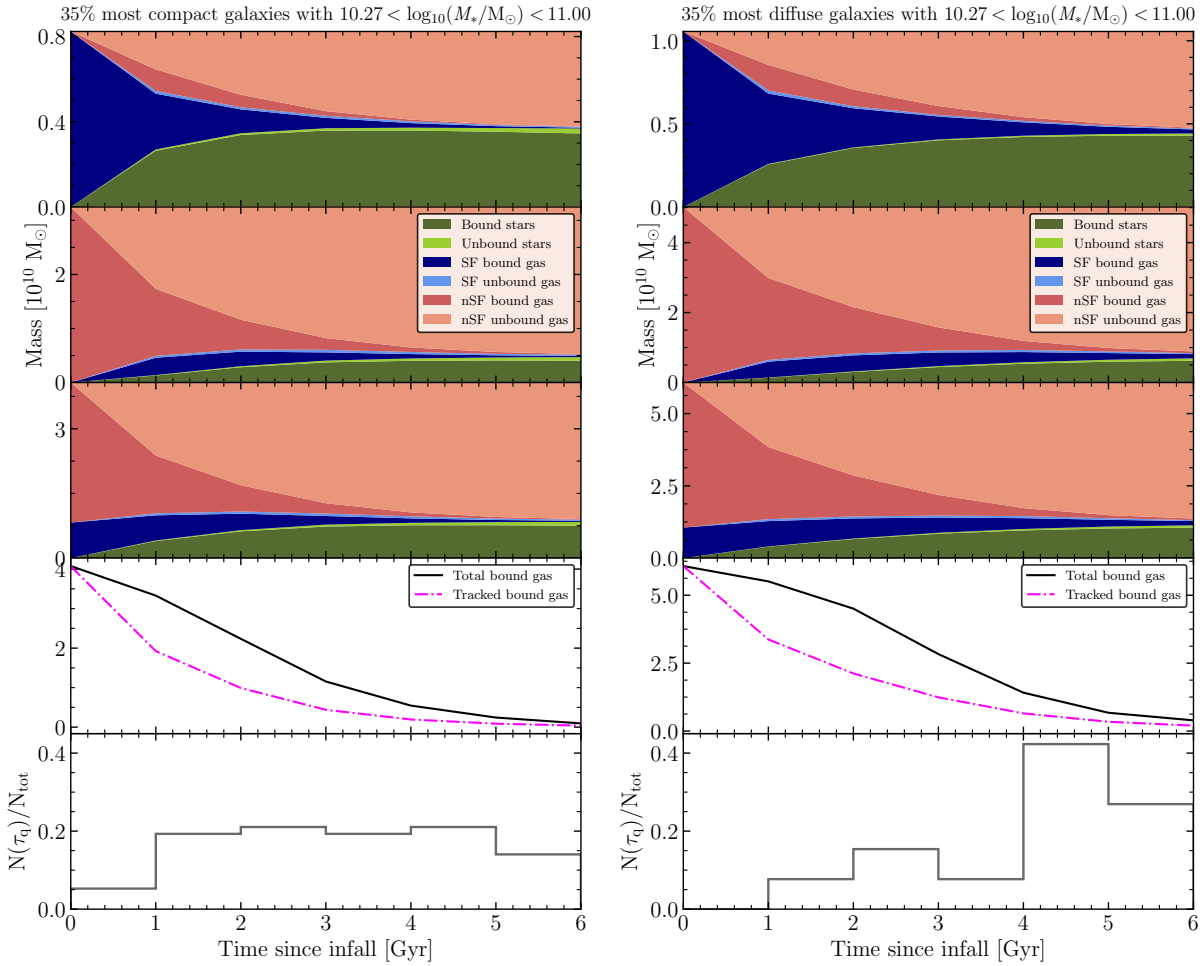

Figure 8: Similar to Figure 4 but for satellite galaxies in the most massive mass bin, *split by* $R_{\star,\mathrm{half}}$ *at* $z = 0$. The colour coding of different mass species is the same as in Figure 4.

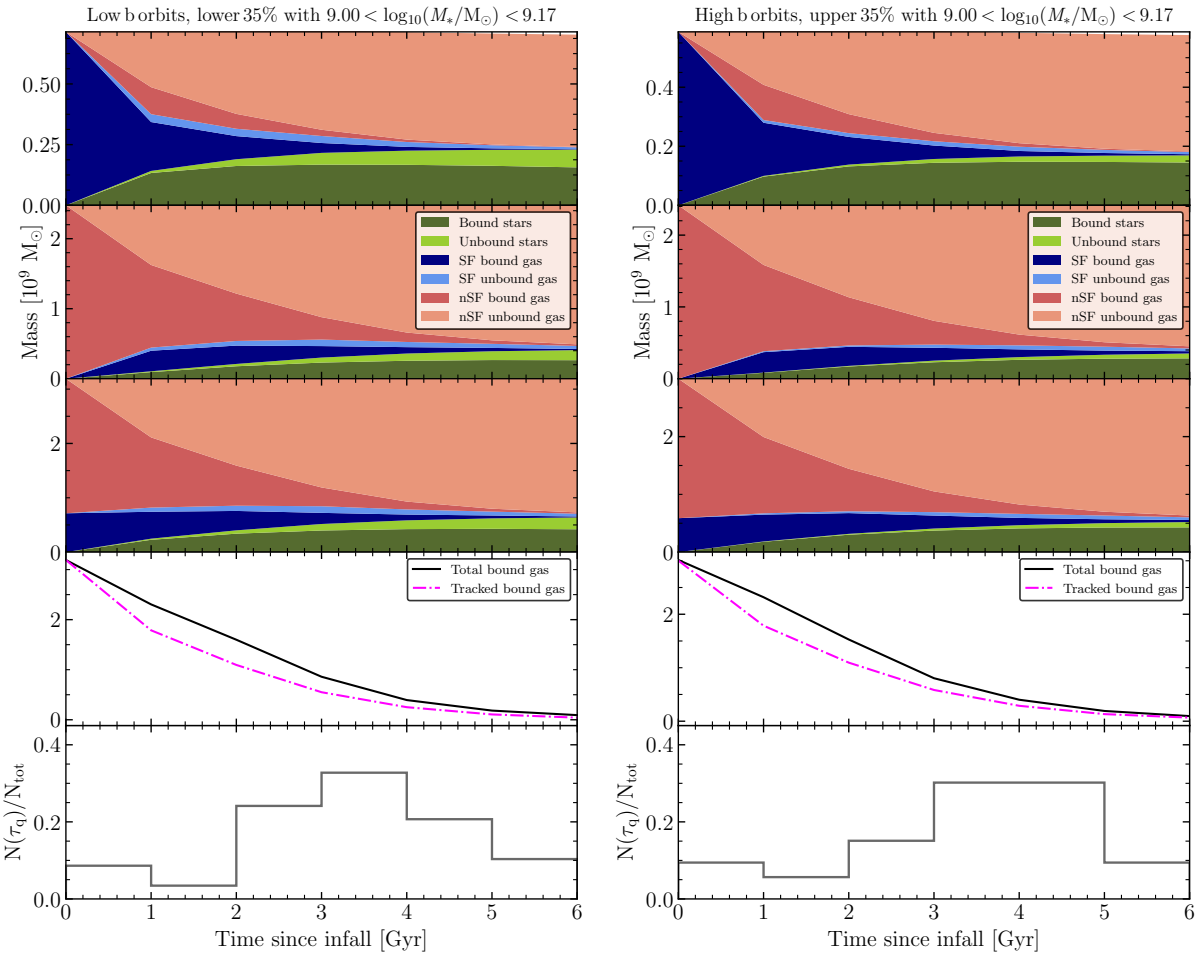

Figure 9: Similar to Figure 4 but for satellite galaxies in the least massive mass bins, *split by impact parameter at* $r_{200,\mathrm{host}}$. The colour coding of different mass species is the same as in Figure 4.

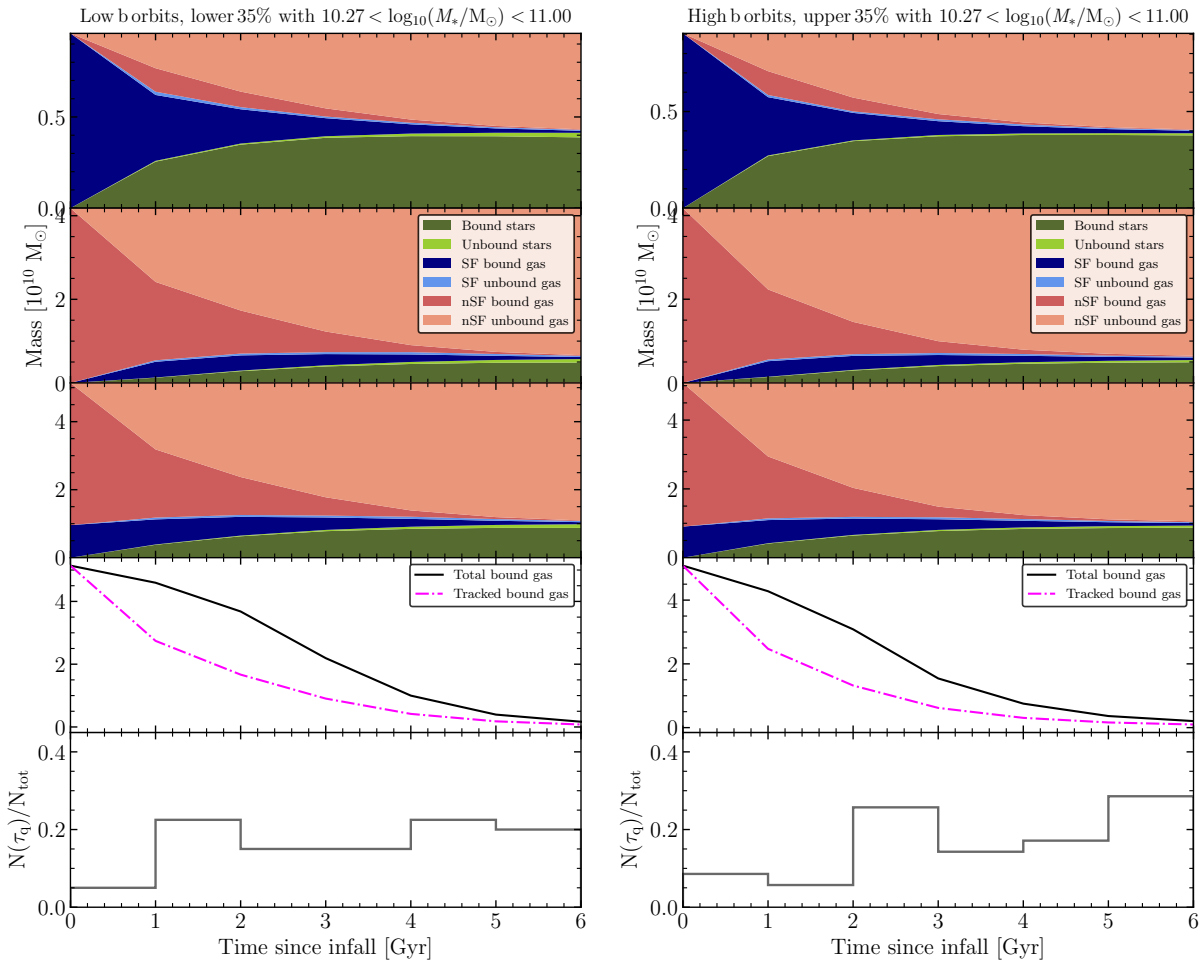

Figure 10: Similar to Figure 4 but for satellite galaxies in the most massive mass bins, *split by impact parameter at* $r_{200,\mathrm{host}}$. The colour coding of different mass species is the same as in Figure 4.

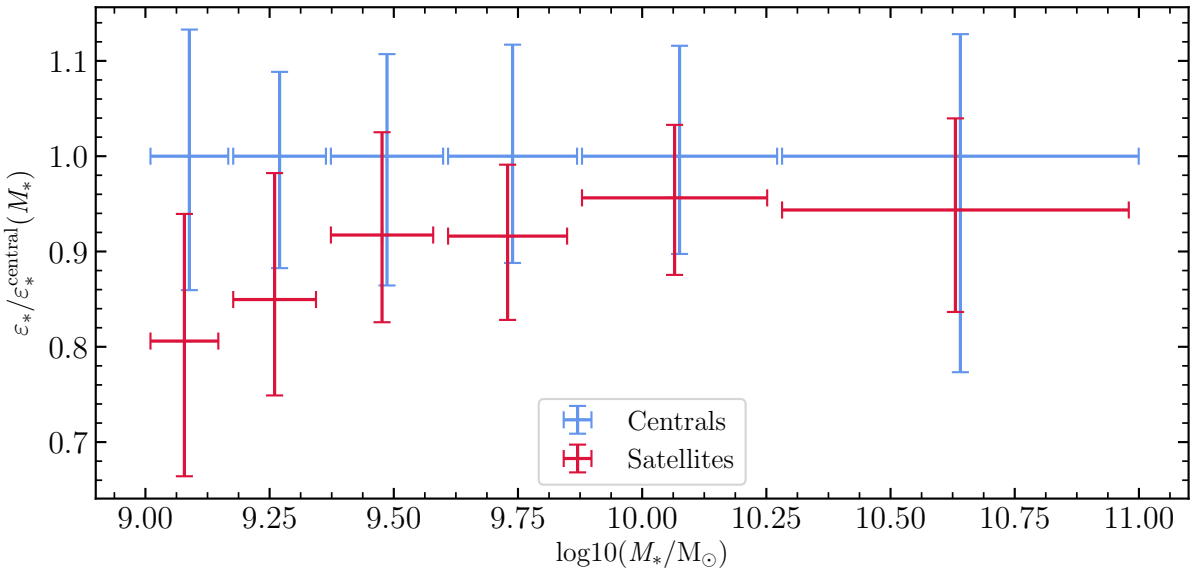

Figure 11: Star formation efficiency (SFE) at $z = 0$, $\varepsilon_\star = \Delta M_\star / M_{\rm gas,c}$ of initially cold gas, normalised by SFE of centrals, $\varepsilon(M_\star)/\varepsilon_{\rm central}(M_\star)$. Red crosses show normalized SFE of satellites and blue crosses show normalized SFE of centrals. SFE of satellites at the low mass end is about 80% of that of the centrals. The SFE of satellites increases with increasing stellar mass to 95% in the highest mass bin. This shows that the effectiveness of the mechanism that removes the cold gas (without consumption) decreases with increasing stellar mass of the satellite. RPS is more effective at halting SF in the low mass satellites than in the high mass satellites (see Section 3.3).

and thus see the differences in the final stellar mass fraction due to environmental effects. The models tried turned out to be too simple and could not capture all the intricate internal and external effects. However, Mitchell and Schaye (2021) have recently published another model that fully describes the stellar-halo mass (SMH) relation of EAGLE galaxies which takes into account gas inflows and outflows. The SMH model has been shown to accurately describe the behaviour of centrals in EAGLE. By setting the pristine accretion terms to 0, it will serve as a model for how the tracked gas would be consumed and expelled by star formation in the absence of environmental effects. By applying it to the tracked gas in satellites and seeing where and how its predictions fail, we can better separate and quantify the role of environment. The reason the SMH model is needed is that it is surprisingly difficult to identify simulation particles impacted by e.g. ram pressure, or by SN feedback. The SMH model looks promising and will be used in the future to fully quantify the environmental effects.

3.4 Halo cooling

We performed a more qualitative examination of initially hot gas (second panels of Figures 4 - 10). Cooling times of hot halos were examined for all galaxies using the cooling tables provided by Wiersma *et al.* (2009a). These cooling functions were used in the making of the EAGLE simulation. They estimate cooling time for gas at a given pressure, temperature, metallicity and redshift. The haloes are large gas reservoirs that are potentially accessible to fuel star formation, if the gas can cool down in a few gigayears. The cooling time for every halo (non-star forming) gas particle was calculated. If the cooling time of a gas particle was calculated to be less that 6 Gyr, then it would be considered potentially accessible for star formation. The mass fraction of

potentially accessible gas for star formation is plotted against stellar mass for each galaxy (log-log plot) and is shown in Figure 12. Low to intermediate mass satellites ($M \approx 10^9 - 10^{10}\,\mathrm{M}_\odot$) have around 1% of their initially hot gas with cooling times longer than 6 Gyr. High mass end galaxies, starting from $M \approx 10^{10.1}\,\mathrm{M}_\odot$ have $\sim 3\%$ of their halo to be inaccessible which increases to $\sim 80\%$ at $M \approx 10^{11}\,\mathrm{M}_\odot$. This is due to higher mass halos having higher virial temperatures T_{vir}.

The peak in quenching timescales (Figure 2) may also be attributed to the fact that galaxies in the 5th mass bin ($M \approx 10^{10}\,\mathrm{M}_\odot$) are at the turn off point, where with growing stellar mass, less and less halo reservoir is accessible to star formation: massive satellites have to rely on the contents of their cold discs to sustain continuous star formation. As mentioned before, more massive galaxies (6th mass bin in Figure 2) have higher SFR and have limited access to their hot reservoirs hence they quench on shorter timescales than the galaxies in the previous mass bin (5th mass bin).

3.5 Cold tails

As galaxies fall into cluster environments, some of their cold gas will be mechanically removed by ram pressure without heating. Cold gas particles that remained cold after being removed from their halo were examined. For each particle at an instance it becomes gravitationally unbound, the distance between the centre of potential of the parent halo and the current position of the particle were recorded. Figure 13 shows the distribution of distances at the moment that cold-remained-cold particles become gravitationally unbound. Positive values are distances to particles that are located in the direction of instantaneous velocity with respect to the host. A plane, perpendicular to the velocity vector and centered at the centre of the potential of the satellite, separates the leading and trailing particles which are represented with positive and negative values, respectively.

The left panel of Figure 13 shows stacked distances to particles over all galaxies and over all snapshots. The asymmetric feature around $D = 0$ ckpc is interpreted as ram pressure that strips cold gas particles which are left behind. Leading particles at large positive distances ($D \gtrapprox 100\,\mathrm{ckpc}$) are, in fact, the particles that were left behind. As the galaxy reaches its apocentre and turns around, its velocity vector points in the direction of earlier stripped particles, resulting in large positive distances of these particles. The panel on the right shows a zoom-in between $-150 < D < 150$ ckpc. The double-peak feature (with the trailing peak being slightly taller and thicker) is the sign of outside-in gas removal. The restoring force in the outer disc region is weaker, hence outer gas particles detach first, which are characterised as leading or trailing by the double-peak feature. There are also tidal effects that will stretch the discs and result in the double peak feature, however tidal stripping is only effective in the inner regions of the host system. Taking the distances of the particles one snapshot after the infall already shows an asymmetric double-peak which can not be attributed to tides at $2.5R_{\mathrm{vir}}$, but can be attributed to RPS and particles that were ejected by SN winds and are left behind. The double peak shows that the average size of the disc is around $\sim 20\,\mathrm{ckpc}$, and illustrates the moment of particles first becoming detached from the outer regions. This effect was observationally shown by Cortese *et al.* 2010 with radial dust deficiency in galaxies of the Virgo cluster.

3.6 Intra cluster light

We examined unbound star particles that were made out of gas which fell in as a part of satellites in order to find a source of intra-cluster light. We looked at all star particles that are not part of the original group at the final snapshot. There is roughly the same amount of formed-then-

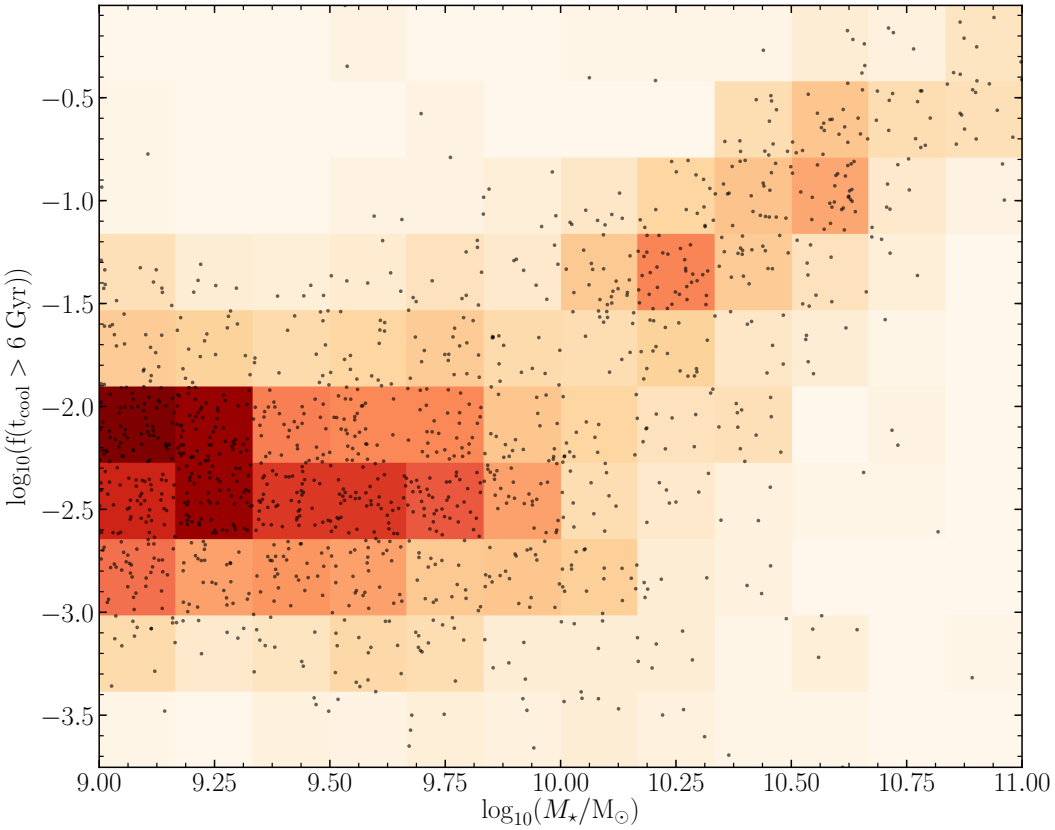

Figure 12: The mass fraction of hot gas that has a cooling time longer than 6 Gyr i.e. a fraction of gas that is not potentially available for star formation. Black dots show values of individual galaxies and the shading is according to the local density of points. There are two distinct populations. One at $M \approx 10^9 - 10^{10}\,\mathrm{M}_\odot$, which has less than $\sim 1\%$ of its gas with $\mathrm{f}(\mathrm{t_{cool}} > 6\,\mathrm{Gyr})$ i.e. almost all of its gas is available for star formation in the next 6 Gyr. There is another population that has an increasing mass fraction of the gas that will not cool in the next 6 Gyr after infall, starting from $\sim 3\%$ at $M \approx 10^{10.25}\,\mathrm{M}_\odot$ and monotonically increasing to $\sim 80\%$ at $M \approx 10^{11}\,\mathrm{M}_\odot$. More massive satellites have fractionally less potentially available gas from their hot reservoirs, so as the mass of the satellite increases they have to rely on the contents of its cold disc to sustain continuous star formation.

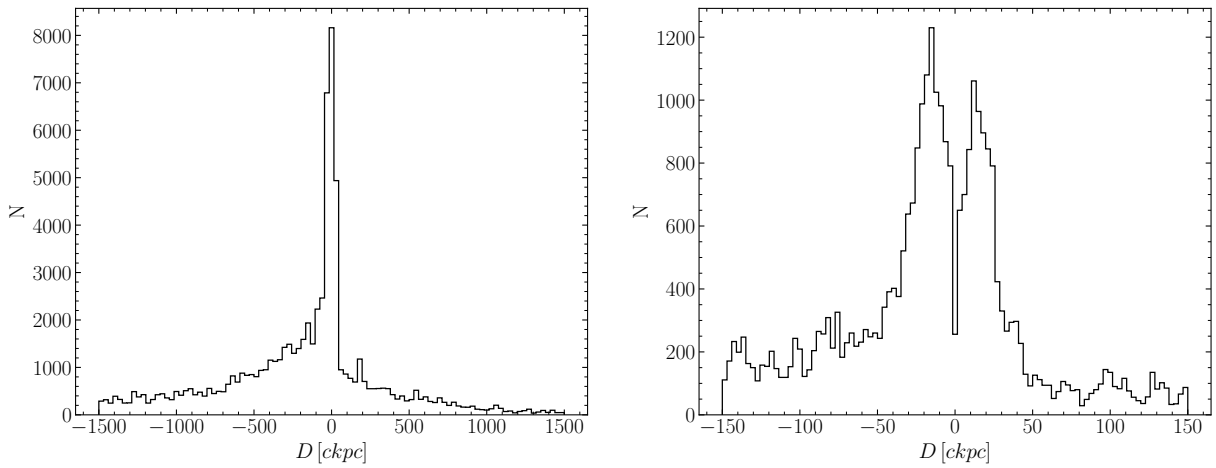

Figure 13: Radial separation of the star forming gas particles that remained star forming at the first snapshot after they became gravitationally unbound from their respective satellite galaxies. The plots show distances of all particles over all snapshots. Positive values show leading particles and negative values show trailing particles. A plane, perpendicular to the instantaneous velocity with respect to the host and centered at the gravitational potential minimum of the satellite divides the space into two subspaces: one with leading particles and one with trailing particles. The left panel shows a clear asymmetric feature, with bins at negative distances having more particles than the ones in front. This is interpreted as the ram-pressure winds stripping the cold particles from satellites. Non-zero positive counts at distances $D \gtrapprox 100$ ckpc are the particles which were left behind ending up "in front" of a satellite after it turns around in its orbit. Leading particles can also be caused by tidal interactions with the host systems in satellites that survive until the pericentric passage. The right panel shows a zoom-in of the inner region $-150 < D < 150$ ckpc. The double peak at $D \approx \pm 30$ ckpc is a sign on outside-in stripping, consistent with observations (Section 3.5). The double peak feature is not visible in the left panel due to coarse binning.

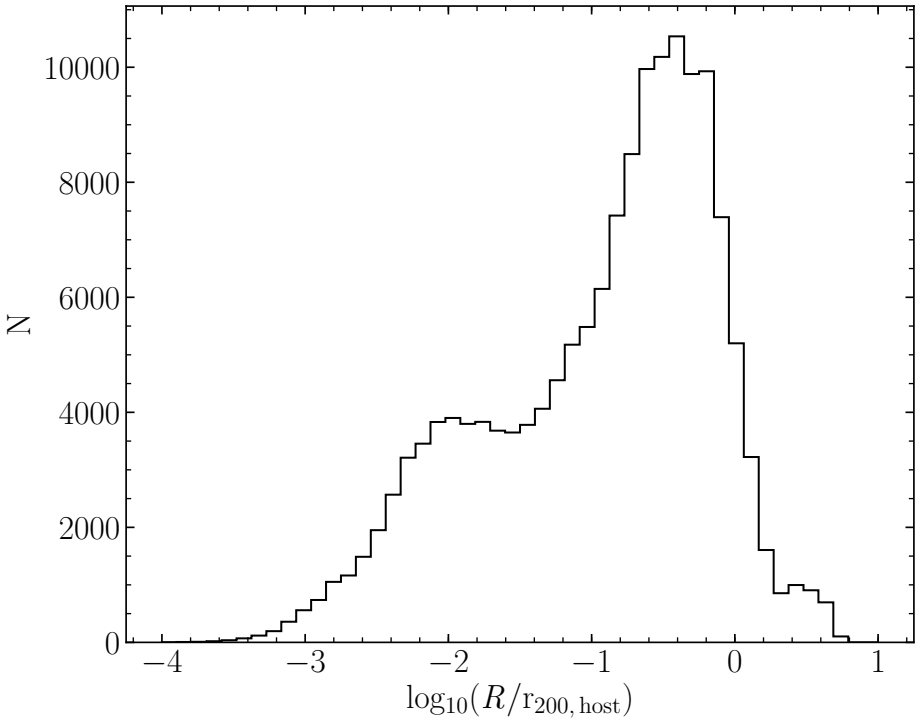

Figure 14: Radial distribution of stripped-then-formed star particles with respect to the centre of the cluster at the moment of their formation. There appear to be two populations at $R/r_{200,\mathrm{host}} \approx 0.3$ and at $R/r_{200,\mathrm{host}} \approx 0.01$ corresponding to stars formed in the ICL (presumably in tails of dense stripped gas) and gas that fell into the central galaxy in the cluster before forming stars there. About a half of star particles that were formed from the gas that was a part of satellites at infall time and are no longer gravitationally bound at the end of the simulation were formed from the gas that was stripped (stripped-then-formed) and another half are tidally stripped star particles (formed-then-stripped). Stars formed from the stripped gas is a substantial source of intra-cluster light in the outer regions of clusters.

stripped and stripped-then-formed star particles. Those which were stripped-then-formed were part for these groups/subhaloes at the next (coarse) time output: 69 % brightest cluster galaxy (BCG) (belongs to the BCG or is part of the group but is not part of any subgroup), 17% is part of another satellite of the cluster (other subhalo but same group), 9% is re-accreted by the same satellite (same subhalo), 5.3% is no longer gravitationally bound to the cluster or its satellites (inside other group or outside any group). This shows that star formation in ram-pressure stripped tails is a rather common occurrence and the stripped-then-formed stars are the source of the intra-cluster light up to R_{200} (~ 1 cMpc) radii of the centre of clusters. Figure 14 shows the radial distribution of stripped-then-formed stars with respect to the centre of cluster in units of $\log10(r/R_{200,\mathrm{host}})$ at the moment of their formation. There appear to be 2 populations: one centered at $0.3R_{200,\mathrm{host}}$, presumably formed in tails or after mass transfer to another satellite and another centered at $0.01R_{200,\mathrm{host}}$, the stripped gas that falls into BCG and is turned into stars there.

3.7 Gas outflows

Mitchell *et al.* (2020) showed that the outflow rates from galactic haloes have a local minimum at $M_{200} \approx 10^{11.7}\,\mathrm{M}_\odot$ or $M_\star \approx 10^{9.7}\,\mathrm{M}_\odot$ at $z < 1.5$, with the outflow rates rising at higher masses due to AGN activity and at lower masses due to SN feedback. The top panels of Figure 4 show that a substantial amount of gas is being expelled in centrals without environmental effects. The same physical mechanisms occur in satellites combined with environment-specific phenomena. All of the effects discussed above in Section 3 contribute to intermediate mass satellites having longer quenching timescales. In satellites at $M_\star = 10^{10}\,\mathrm{M}_\odot$, the lower outflow rates, combined with fully accessible halo gas (section 3.4) and no further accretion after infall provides a reasonable explanation of the peak in the quenching timescales: galaxies at this mass have higher $M_{\mathrm{gas}}/\mathrm{SFR}$ with higher gas mass available for the star formation and they have weakest negative feedback out of all galaxies in the mass range $10^9 < M_\star/\mathrm{M}_\odot < 10^{11}$.

4 Discussion

In this section we compare our results to recent studies in the field, both observational and numerical and discuss how different definitions of the same property for example, t_{inf}, may affect the interpretation.

4.1 Binning and selection effects

We begin by discussing how different binning approaches of galaxies may be appropriate in different studies. For this work binning satellite galaxies by their final stellar mass at $z = 0$ was chosen in order to have a meaningful comparison with observational results from other studies of the nearby Universe. Final stellar mass of galaxies is an observable property of satellites as they fall into clusters and evolve while interacting with the dense environment.

Satellites, however, can also be binned by their stellar mass at infall time. This would allow for comparison of galaxies that have very similar properties before the infall, rather than at $z = 0$. Figure 15 shows such binning (black crosses) plotted against the binning by final stellar mass. Overall, the trend of intermediate mass satellite having longer quenching timescales is preserved, with a very minor increase in quenching time in the lowest mass bin. As satellites continue their SF, they will all gain approximately the same amount of stellar mass (25-40% of their infall mass) in respective mass bin, such that, for example, a satellite in the most massive mass bin at infall will remain in the same mass bin at the end of the simulation. Occasionally, some galaxies will produce more stars than usual, or lose a substantial fraction of their stellar mass by the end of the simulation, which would make galaxies "jump" mass bins. The binning can be done by orbital properties (impact parameter and anisotropy parameter), host mass, gas content or infall time, all depending on the main focus of the study.

We have chosen 6 stellar mass bins of equal galaxy counts in each bin. This selection is not "special" compared to higher and lower mass bin counts as all of them will show a peak in quenching timescales at intermediate masses. Likewise, evenly spaced bin widths of set width on log scale show an identical trend. One caveat is that there is a much lower satellite count of masses $\mathrm{M}_\star > 10^{10}\,\mathrm{M}_\odot$ than $\mathrm{M}_\star < 10^{10}\,\mathrm{M}_\odot$, which would result in $\lesssim 30$ satellites in the highest mass bin at $10^{10.75} < \mathrm{M}_\star/\mathrm{M}_\odot < 10^{11}$, compared to ~ 500 in the $10^{9} < \mathrm{M}_\star/\mathrm{M}_\odot < 10^{9.25}$ mass bin. This would hinder the statistical approach.

Lastly, in our $\tau_\mathrm{q} - M_\star$ relations (Figures 2 and 3) we have selected satellites that quench after infall. This approach allowed us to have very similar (± 1 galaxy) counts in each mass bin. However, it introduced a bias towards galaxies that are prone to be quenched. i.e. gas poor galaxies, low impact parameter galaxies diffuse low mass satellites and compact high mass satellites. Future work will have to account for this and include all satellites, even those which do not quench by $z = 0$. The full sample is representative of all interactions, including those which do not result in quenching events but are still a part of a satellite population. We note that in the mass partition plots all galaxies (quenched and not quenched by $z = 0$) are taken into account for the analysis.

4.2 Background effects of gas that was not tracked on centrals and satellites

As mentioned in Section 3.2.1, we selected a reference sample of central satellites in order to compare them to satellites and observe how environmental effects would change the mass evolution of satellites. Since only one snapshot worth of gas particles was tracked, any other further accretion and any effects of newly accreted gas (referred to as "background gas") on the tracked gas was ignored. The background gas contributed to the increased gas density in the star forming

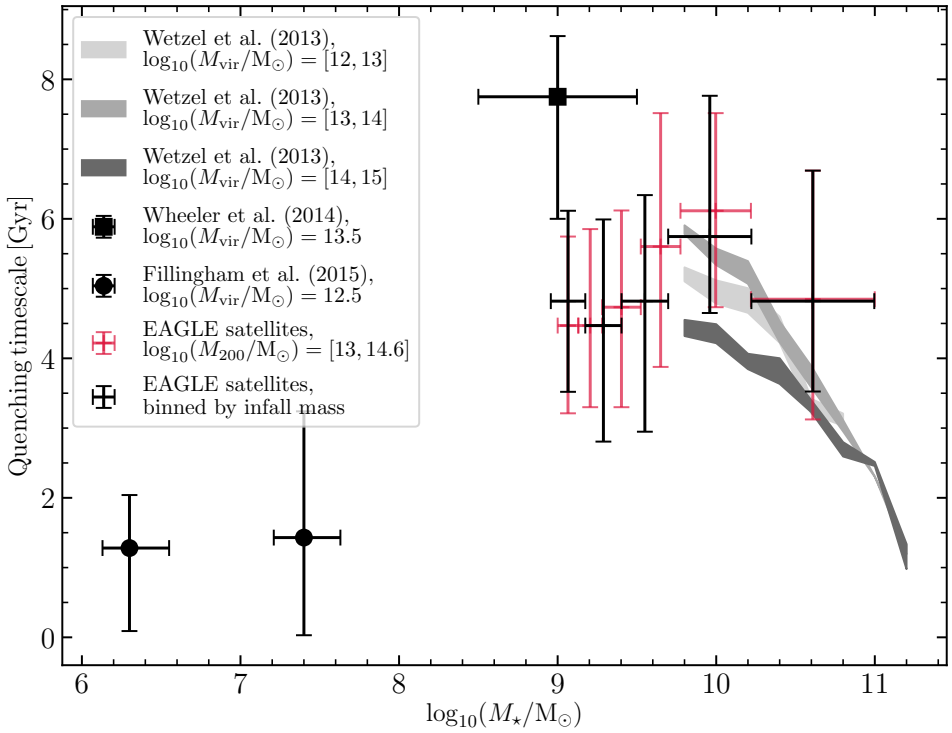

Figure 15: Quenching timescale as a function of satellite stellar mass. Same as Figure 2 but with added binning by stellar mass at infall time (black crosses) for comparison. Binning by infall stellar mass and by stellar mass at $z = 0$ yield very similar results.

regions, which in turn would increase instantaneous SFR. This would lead to faster gas depletion compared to the case where there would not be any further accretion (i.e. a very isolated galaxy).

By the same token, stars formed from the background gas would contribute to the background SN winds and heating, which would heat up and expel the tracked gas that would otherwise not be heated nor expelled. This effect would decrease SFR of a galaxy but could also deplete the gas reservoirs. In addition, it can remove/heat up star forming gas or remove the hot gas that otherwise would have cooled down. It is unclear what the net effect of background heating and SN winds is on quenching timescales would be, but it is clear that it would be different to a galaxy that evolves in complete isolation, without any further gas accretion. It is not clear how the combined effect of increase in background density, increase in background winds and heating affects the tracked gas, since these two are competing effects that reduce and increase SFR.

4.3 Comparison to observations

We now compare observational experiments with our results in order to assess if and how well they describe the observed Universe. In many cases, different authors use different definitions that fit their approach best, so it is not trivial to compare results: one must take into the consideration how these different definitions will affect the outcome of a particular study. Also, we remind the reader that a galaxy that is quenched at redshift $z_{\rm quench}$ has fallen in its host environment at least 1 quenching timescale ago.

We remind the reader that the results of the studies displayed in Figure 2 or 15 were obtained using different definition of infall times and were performed around different host masses,

therefore those results must be interpreted qualitatively.

Before we turn the reader's attention to other studies in the field, we first want to revisit the results of W13 (Figure 2 or 15). They studied evolution of massive $M_\star > 10^{10}\,M_\odot$ satellite galaxies in the nearby ($z \approx 0$) Universe. The authors used Sloan Digital Sky Survey Data Release 7 and N-body simulation to track satellite orbits and infer satellites' infall time t_{infall}; they define t_{inf} as the first time when a galaxy crosses R_{vir} of their host halo. The most relevant result to this thesis is that quenching timescales of satellite galaxies decrease with increasing stellar mass and are independent of host mass. W13 quenching timescales are shorter than the ones we find, but this is due to their infall radius being R_{vir} while ours is $2.5R_{vir}$. It takes slightly longer than 1 gigayear for a satellite galaxy to traverse from $2.5R_{vir}$ to $1 \times R_{vir}$, which is exactly the difference between our results and that of W13. This indicates that our simulation results are consistent with observational studies. Splitting the sample by host mass, however, yields shorter timescales for for satellites around more massive hosts, which contradicts the conclusion of W13. This may be attributed to RPS being too efficient at removing gas particles from infalling galaxies, as ram pressure exerted by the environment on a satellite is proportional to the density of the environment. Since more massive hosts have denser environments, RPS in EAGLE may remove the cold gas even in high mass satellites. There is also a possibility that the denser environment pressurises the gas in the disc of the infalling high mass galaxies such that cold gas is consumed by enhanced SFR or shorter timescales. Effects of higher density environments can be investigated in more detail in future work.

4.3.1 Lemaux *et al.* (2019)

Lemaux *et al.* (2019) (L19 hereafter) studied the relationship between the galaxy colour and galaxy density from Observations of Redshift Evolution in Large Scale Environments (ORELSE) a survey in redshift range $0.55 \leq z \leq 1.4$. In this study, infall time is set to time at which galaxy joins a group/cluster (same as W13) and quenching time is when a galaxy joins the quenched region in the $NUVrJ$ diagram. The infall time was set by orbit matching with N-body simulation. The quenching timescale for galaxies in 2 mass bins of $\log(< M_\star > /M_\odot) = 10.26$ and $\log(< M_\star > /M_\odot) = 10.9$ are $3.3 \pm 0.3\,\mathrm{Gyr}$ and $2.4 \pm 0.3\,\mathrm{Gyr}$, respectively. It has been established that harassment and RPS could not be responsible for quenching as they continued SF activity for 0.5-1.5 gigayearsr after pericentic passage. Thus these galaxies must have been quenched by other environmental mechanisms. This is a consistent result with the work of W13 and this thesis in a sense that τ_q decreases with increasing stellar mass and that starvation is the main quenching mechanism in the mentioned stellar mass range. Comparing the values of τ_q of L19 to the results of W13 in Figure 2, the quenching time of galaxies in L19 is shorter, but this is to be expected since SFR of galaxies in mass range $\log_{10}(M_\star/M_\odot) = [10, 11]$ has dropped by a factor of ~ 10 from $z = 1$ to $z = 0.2$ (Karim *et al.* 2011), while molecular gas mass fraction increases by a factor of ~ 2.5 of over the same redshift range (Tacconi *et al.* 2018). This means that depletion timescales $\tau_{dep} = M_{gas}/SFR$ will be shorter at higher redshifts, given the molecular gas is not replenished or is replenished at the same rate at all respective redshifts (Upadhyay *et al.* 2021). Since starvation is closely related to depletion timescales, quenching by starvation at $z = 1$ would yield shorter quenching timescales. The infall time in L19 is set to the time when a galaxy becomes part of a group, i.e., at the time of crossing R_{vir} of its host halo. This would result in overall shorter quenching timescales, compared to our quenching timescales, as galaxies are being tracked from closer radial separation from their host. We remind the reader that our infall radius is set to $2.5R_{vir}$, hence our quenching timescales are expected to be a few gigayers longer, as is the case.

4.3.2 Haines *et al.* (2015)

Next, we examine the study of Haines *et al.* (2015) (H15 hereafter), who studied 30 massive clusters at $0.15 < z < 0.3$ in X-ray to NiR photometric bands. They show that the fraction of star forming galaxies ($\mathrm{SFR_{IR}} > 2.0\,\mathrm{M_\odot\,yr^{-1}}$) of massive satellite galaxies ($M > 2.0 \times 10^{10} M_\odot$) increases with projected cluster-centric radius and is about 1/3 lower at $r_{\mathrm{proj}}/r_{500}$, compared to field galaxies at that redshift. By stacking and matching orbits from 75 most massive clusters in the Millennium simulation (Springel *et al.* 2005b) the authors concluded that massive satellites are quenched by a slow process on timescales of $t_q = 1.73 \pm 0.25\,\mathrm{Gyr}$ upon accretion (crossing of r_{200}). With cluster masses $\log(\mathrm{M_{500}/M_\star}) \approx [14, 15]$, these results align quite well with those of W13 around most massive host systems, $\log(\mathrm{M_{vir}/M_\star}) = [14, 15]$ (Figure 2). As mentioned before, SFR of galaxies at $0.15 < z < 0.3$ was a few times higher than that of galaxies and molecular gas mass fraction was almost the same at $z = 0$, which would make the depletion timescales shorter and hence quenching timescales would also be shorter at higher redshifts.

The slow quenching process and a rather low quenching timescales at high stellar masses is consistent with results of this thesis, although the τ_{q} values likely differ due to different definitions of infall time. H15 defines infall times as time of crossing of $\mathrm{r_{200}}$ and our definition of infall is the crossing of $3.3 \times \mathrm{r_{200}}$, hence by construction, our quenching timescales will always be longer by about 1.5 Gyr, as galaxies have to travel longer distances until their individual quenching times come. Likewise, their definition of a star forming galaxy is by $\mathrm{SFR_{IR}} > 2.0\mathrm{M_\odot yr^{-1}}$, which would also make quenching timescales slightly shorter than those calculated from our definition. Accounting for the differences in the definitions of infall and quenching time, results of H15 are within the interquartile range of the results of this work.

4.3.3 Boselli *et al.* (2016)

Boselli *et al.* (2016) (B16 hereafter) analysed K-band selected galaxies from Herschel Reference Survey. 322 nearby ($15 \leq \mathrm{D} \leq 25\,\mathrm{Mpc}$) galaxies of stellar mass $10^8 < \mathrm{M_\star/M_\odot} < 10^{11}$ were selected, which comprise a representative sample of the local universe population that resides in a diverse range of densities: from the core of the Virgo cluster, to small groups and isolated field objects. B16 used spectral energy distribution (SED) fitting to reconstruct galaxies' star formation histories in order to estimate their quenching times. Their SED fitting for HI-deficient galaxies worked better when they assumed a truncated star formation history, a model which assumes removal a large fraction of cold gas by the galaxy's hostile immediate environment. Furthermore, a fraction of satellites that reduce their star formation by 80% decreases by a factor of ~ 5 from the core of the Virgo cluster ($\mathrm{R/R_{vir}} < 0.5$) to the outskirts ($\mathrm{R/R_{vir}} \geq 4$). HI-deficient objects were estimated to fully stop their star formation activity 1.3 Gyr ago from now via RPS. Results of B16 contradict the findings of this work regarding the main quenching mechanism at stellar masses $\mathrm{M_\star/M_\odot} > 10^9$. Since the results should be compared qualitatively, we compare the quenching mechanisms of EAGLE galaxies and observed galaxies above their characteristic masses $\mathrm{M_c}$ ($\mathrm{M_\star/M_\odot} = 10^8$ for observed galaxies and $\mathrm{M_\star/M_\odot} = 10^{10}$ for EAGLE galaxies). We conclude that the galaxies that are more massive than $\mathrm{M_c}$ are quenched via starvation. However, if a massive galaxy survives long enough to swing around pericenter, RPS will play a big role is stripping of star-forming gas as $\mathrm{P_{RPS}} \approx \mathrm{v^2}\rho_{\mathrm{ICM}}$. The satellite galaxy will have a maximum velocity and will be traversing the densest regions of its environment. Additionally, B16 use a different definition of quenching times. They define it as lookback times to quenching epochs, which is a completely different definition to our quenching timescales. In order to make a quantitative comparison between the results of B16 and this work, one would need to calculate infall time for every galaxy in B16's study to infer quenching timescales.

4.4 Context and simulation performance (RPS)

We now compare our results to the results of other works that attempted to quantify quenching timescales as a function of stellar mass in satellites in different simulations.

4.4.1 Wright *et al.* (2019)

Wright *et al.* (2019) mesurements of quenching timescales in EAGLE satellites differ from our definition in two ways: (i) time it takes for a satellite to cross the green valley in the colour mass diagram, that is, time taken between departure form the blue cloud and arriving to the red sequence (they used $u^* - r^*$ colours); (ii) leaving main sequence and arriving on the passive cloud of the SSFR-mass relation (SSFR $< 10^{-11}\,\mathrm{yr}^{-1}$). Around 93% of galaxies overlap between these two definitions. These authors used integrated properties of simulated galaxies only and thus have a set of results that can be compared against ours. In the stellar mass range of $10^9 < \mathrm{M}_\star/\mathrm{M}_\odot < 10^{11}$ quenching timescales of low mass satellites increases up to a stellar mass of $\mathrm{M}_\star \approx 10^{10}\mathrm{M}_\odot$ and decreases at higher stellar masses for both of their definitions. Satellites below $\mathrm{M}_\star < 10^{9.6}\mathrm{M}_\odot$ are quenched by RPS and those above $\mathrm{M}_\star > 10^{10.3}\mathrm{M}_\odot$ are quenched by AGN activity and behave in a similar way to central galaxies. All of the above conclusions of Wright *et al.* (2019) (except the high mass satellites are quenched by AGNs) are consistent with the finding of this work, which is not surprising, given the same simulations were used in both studies.

4.4.2 Akins *et al.* (2021)

Another simulation that we compare our results against is DC Justice League (DCJL) suite (Akins *et al.* 2021), which is a set high resolution zoom-in simulations of the Local Group size galaxies. These simulations accurately reproduce satellite luminosity function. The mass resolution is $4.2 \times 10^4\,\mathrm{M}_\odot$ for dark matter particles, $2.7 \times 10^4\,\mathrm{M}_\odot$ for gas particles and star particles begin with masses of $8000\mathrm{M}_\odot$ (compared to $1.8 \times 10^6 M_\odot$ of EAGLE particles); force softening length is 170 pc (compared to 700 pc in EAGLE). Cooling and heating of gas is included. Star formation is determined probabilistically, set by H_2 abundances, their temperatures and densities. The infall time is defined by a satellite crossing of $\mathrm{R}_{\mathrm{vir}}$ of its host system and quenching is defined by the by time at which SSFR reaches 0 or $10^{-11}\,\mathrm{yr}^{-1}$. Their work aligns very well with the work of F15 in terms of host masses and usage of the same definitions of infall and quenching times. Akins *et al.* (2021) find that galaxies below characteristic stellar mass of $\mathrm{M}_\star = 10^8\mathrm{M}_\odot$ are quenched rapidly by RPS with gas poor galaxies quenching more rapidly than gas rich galaxies. Above the characteristic stellar mass, galaxies can effectively resist RPS. The conclusion is also similar to ours, but we find characteristic mass at $\mathrm{M}_\star = 10^{10}\mathrm{M}_\odot$. This may be due to spatial resolution of EAGLE, which is 5 times smaller than that of DC Justice League. This would result in rather aggressive RPS, which would move the characteristic mass to higher values, since deeper potential wells are needed to resist RPS effectively, as is the case with our results.

4.4.3 Mistani *et al.* (2016)

The last study we compare our results to is the work done by Mistani *et al.* (2016). Using ILLUSTRIS simulation, they studied how cluster environments affect formation of dwarf ellipticals and globular clusters. They also measured quenching timescales as a function of stellar mass in infalling galaxies. ILLUSTRIS, overall, is a similar cosmological simulation to EAGLE in terms of simulation box size and mass resolution, however it has some very notable differences. The largest difference is that fluid elements live on an unstructured moving mesh, compared to meshfree

smoothed particle hydrodynamics method used in EAGLE. Softening length is at most 700 kpc (similar to that of EAGLE) but it can be as low as 48 pc. The Authors found similar quenching timescales to ours, peaking at $M_\star = 8 \times 10^9\,\mathrm{M}_\odot$ and decreasing at lower and higher masses. They defined the infall time as time at which the dwarf galaxy reached its maximum mass, which would typically be the moment right before or at the moment of entering dense cluster environment. Our definition of infall radius being $3.3R_{200}$ is almost the same, as maximum mass of satellites is reached right before or at the point of infall. This can be seen from the total bound mass decreasing with time (there must have been a maximum mass before infall) in 4th panels from the top of Figures 4 - 8. Quenching time was determined by SSFR dropping below $10^{-11}\,\mathrm{yr}^{-1}$. While the absolute values of quenching time differ slightly, the trend of intermediate mass satellite having longer quenching timescales is recovered. Seemingly different approaches to define the infall time (one is defined through the internal properties of the satellites and the other by the properties of the environment) yield very similar results because the internal properties of the satellites is set by the interaction with its environment.

The three simulations ILLUSTRIS, EAGLE and DCJL agree on the fact that there is a peak in quenching timescales in satellite galaxies at intermediate masses, however only two of them (ILLUSTRIS and EAGLE) agree with each other where the peak occurs. This may be due to limiting spatial resolution which promotes more aggressive RPS. DCJL, having a 5x the spatial resolution of ILLUSTRIS and EAGLE much better reproduce the derived quenching timescales of satellites around MW. If it is the case, the next generation cosmological simulation COLIBRE that will have $\sim$ 64x mass resolution and $\sim$ x4 spatial resolution of EAGLE, will have the peak at lower masses.

5 Conclusion

In this thesis we studied the main quenching mechanisms of satellite galaxies in the EAGLE simulation and the origin of the peak in the $\tau_q - M_\star$ relation. We selected satellite galaxies before the moment they fall into a cluster ($3.3 \times R_{200,host}$) and track their gas particles until the end of the simulation. The points below summarize the main results of this thesis:

- The characteristic mass M_c of satellites in EAGLE is at $\log_{10}(M_\star/M_\odot) = 10 \pm 0.2$. This is due to several effects: (i) M_c is still at the mass where virial temperature of the hot halo is low enough to have cooling times less than 6 gigayears, which makes the hot reservoir potentially accessible for future star formation; (ii) SFR decreases with stellar mass, so more potentially available gas at lower SFR will result in longer depletion timescales $\tau_{depl} = M_{gas}/SFR$; (iii) satellites at these masses start to resist RPS effectively due to them having deep potential wells; (iv) there is a local minimum in the outflow rate at M_c, with outflow rates rising due to AGN activity at higher masses and due to SN feedback at lower masses.

- Satellites with masses below M_c are quenched mainly by RPS and with masses above M_c, by starvation. It was inferred from star formation efficiency of cold gas in satellite galaxies and from splitting the population by their size ($R_{half,\star}$) that: (i) low mass compact satellites take *longer* to quench than their diffuse counterparts, presumably compact galaxies can resist RPS more effectively as they have deeper potential wells hence they can produce stars for longer times; (ii) high mass compact satellites quench more quickly than their diffuse counterparts, presumably because the deeper potential wells can pressurize gas more effectively leading to higher SFRs at similar gas mass fractions (compared to diffuse massive satellites), hence they deplete their cold reservoirs faster.

- RPS in EAGLE is likely too effective, putting the characteristic mass at $\log_{10}(M_\star/M_\odot) \approx 10$, while observations suggest that M_c is at $\log_{10}(M_\star/M_\odot) \approx 9$. The observations at the low mass end trace quenching timescales in groups of galaxies. Zoom-in simulations around MW-lie galaxies suggest that M_c is at $\log_{10}(M_\star/M_\odot) \approx 8$. Given that environmental effects are weaker in groups, compared to clusters, the true M_c in clusters must be somewhere between $\log_{10}(M_\star/M_\odot) = (8, 10)$.

- Star formation continues in ram-pressure stripped tails; RPS is an outside-in process: outer regions of the cold disc are stripped first.

- The intra-cluster light in clusters comes from roughly equal parts formed-then-stripped and stripped-then-formed stars. The majority of the stars that were formed from the gas that fell into the cluster as a part of a galaxy will end up between $0.1\,R_{200}$ and R_{200} in the cluster.

A useful extension of this work would be the usage of a stellar-halo mass model, developed by Mitchell and Schaye (2021) that was specifically built to describe stellar mass growth of EAGLE galaxies. After being fit to describe central galaxies this model would help infer how SFHs of satellites differ from centrals as a function of stellar mass giving insight into the particular physics affecting satellites .

Another improvement would be to include galaxies that do not quench by $z = 0$ in $\tau_q - M_\star$ plots. This would remove any biases towards orbital and internal properties that favour quenching to occur.

Next, for consistency and ease of comparison with the observational results, a separate analysis of quenching timescales with infall times at $1R_{\rm vir}$ or R_{200} can be performed.

Quantifying precisely how AGN and SN winds impact the gas cycle would greatly improve our understanding of where the effects of winds end and where the ram pressure starts to affect the satellite galaxy.

Finally, since next generation cosmological simulations are around the corner (e.g. COLIBRE, EAGLEXL) it would be relatively easy to use the same approach or even code to see how their physics reproduces ram-pressure effects, compared to observations. If spatial resolution is indeed the main factor that determines the position of the peak in the $\tau_{\rm q} - M_\star$ relation, higher resolution simulations should have the peak at lower masses.

With this study we attempted to describe how cold gas in EAGLE satellites is affected by its dense environment as a function of their stellar mass. The quenching mechanisms seem to work together. This is the first study where individual gas particles were tracked in the EAGLE simulation in order to isolate the environmental effects of their environments on satellites. Our approach paves the way for future studies to extract as much insight on the role of environment in galaxy evolution as possible from the rich data sets provided by modern cosmological hydrodynamical simulations.

Acknowledgements

I thank my supervisor Kyle Oman for countless discussions and explanations, for swift responses and for offering to carry out this research in the first place. I thank my other supervisor, Marc Verheijen for valuable feedback and research ideas. My eternal gratitude to Callum Blair, Eva Visser and Olga Zadvorna for the thesis script revision. I thank Jan Oort for lifting my spirit when my morale was low. Finally, I thank the COSMA group for providing me access to their computational facilities. This work used the DiRAC@Durham facility managed by the Institute for Computational Cosmology on behalf of the STFC DiRAC HPC Facility (www.dirac.ac.uk). The equipment was funded by BEIS capital funding via STFC capital grants ST/K00042X/1, ST/P002293/1, ST/R002371/1 and ST/S002502/1, Durham University and STFC operations grant ST/R000832/1. DiRAC is part of the National e-Infrastructure.

References

1. H. B. Akins *et al.*, *ApJ* **909**, 139 (Mar. 2021).
2. J. Arthur *et al.*, *MNRAS* **484**, 3968–3983 (Apr. 2019).
3. Y. M. Bahé, I. G. McCarthy, M. L. Balogh, A. S. Font, *MNRAS* **430**, 3017–3031 (Apr. 2013).
4. I. K. Baldry *et al.*, *ApJ* **600**, 681–694 (Jan. 2004).
5. W. A. Baum, **71**, 106–117 (Apr. 1959).
6. A. F. L. Bluck *et al.*, *MNRAS* **499**, 230–268 (Nov. 2020).
7. A. F. L. Bluck *et al.*, *MNRAS* **462**, 2559–2586 (Nov. 2016).
8. A. Boselli *et al.*, **596**, A11 (Nov. 2016).
9. S. Brownson, F. Belfiore, R. Maiolino, L. Lin, S. Carniani, *MNRAS* **498**, L66–L71 (Nov. 2020).
10. G. L. Bryan, M. L. Norman, *ApJ* **495**, 80–99 (Mar. 1998).
11. H. Butcher, J. Oemler A., *ApJ* **285**, 426–438 (1984).
12. R. K. Cochrane, P. N. Best, *MNRAS* **480**, 864–878 (Oct. 2018).
13. C. A. Correa, J. Schaye, J. W. Trayford, *MNRAS* **484**, 4401–4412 (Apr. 2019).
14. L. Cortese, B. Catinella, R. Smith, *arXiv e-prints*, arXiv:2104.02193 (Apr. 2021).
15. L. Cortese *et al.*, **518**, L49 (July 2010).
16. K. Dolag, S. Borgani, G. Murante, V. Springel, *MNRAS* **399**, 497–514 (Oct. 2009).
17. M. Donnari *et al.*, *MNRAS* **500**, 4004–4024 (Jan. 2021).
18. A. Dressler, *ApJ* **236**, 351–365 (1980).
19. D. Elbaz *et al.*, **468**, 33–48 (June 2007).
20. S. P. Fillingham *et al.*, *MNRAS* **454**, 2039–2049 (Dec. 2015).
21. J. E. Gunn, I. Gott J. Richard, *ApJ* **176**, 1 (1972).
22. C. P. Haines *et al.*, *ApJ* **806**, 101 (June 2015).
23. L. Jiang, J. C. Helly, S. Cole, C. S. Frenk, *MNRAS* **440**, 2115–2135 (May 2014).
24. A. Karim *et al.*, *ApJ* **730**, 61 (Apr. 2011).
25. R. B. Larson, B. M. Tinsley, C. N. Caldwell, *ApJ* **237**, 692–707 (1980).
26. J. Lee *et al.*, *ApJ* **905**, 31 (Dec. 2020).
27. B. C. Lemaux *et al.*, *MNRAS* **490**, 1231–1254 (Nov. 2019).
28. M. Lotz, R.-S. Remus, K. Dolag, A. Biviano, A. Burkert, *MNRAS* **488**, 5370–5389 (Oct. 2019).
29. G. A. Mamon, T. Sanchis, E. Salvador-Solé, J. M. Solanes, **414**, 445–451 (Feb. 2004).
30. Y.-Y. Mao *et al.*, *ApJ* **907**, 85 (Feb. 2021).
31. S. McAlpine *et al.*, *AC* **15**, 72–89 (2016).
32. P. A. Mistani *et al.*, *MNRAS* **455**, 2323–2336 (Jan. 2016).
33. P. D. Mitchell, J. Schaye, *arXiv e-prints*, arXiv:2103.10966 (Mar. 2021).

34. P. D. Mitchell, J. Schaye, R. G. Bower, R. A. Crain, *MNRAS* **494**, 3971–3997 (May 2020).
35. H. Mo, F. van den Bosch, S. White, *Galaxy Formation and Evolution* (Cambridge, 2010).
36. R. Morganti, *Frontiers in Astronomy and Space Sciences* **4**, 42 (Nov. 2017).
37. K. Morokuma-Matsui *et al.*, *arXiv e-prints*, arXiv:2103.05867 (Mar. 2021).
38. K. A. Oman *et al.*, *MNRAS* **501**, 5073–5095 (Mar. 2021).
39. J. H. Oort, *A&A* **7**, 381 (1970).
40. Planck Collaboration *et al.*, *A&A* **571**, A1 (2014).
41. M. Postman, M. J. Geller, *ApJ* **281**, 95–99 (1984).
42. I. D. Roberts *et al.*, *arXiv e-prints*, arXiv:2106.06315 (June 2021).
43. Y. M. Rosas-Guevara *et al.*, *MNRAS* **454**, 1038–1057 (Nov. 2015).
44. L. V. Sales *et al.*, *MNRAS* **447**, L6–L10 (Feb. 2015).
45. J. Schaye, *ApJ* **609**, 667–682 (July 2004).
46. J. Schaye, C. Dalla Vecchia, *MNRAS* **383**, 1210–1222 (Jan. 2008).
47. J. Schaye *et al.*, *MNRAS* **446**, 521–554 (2015).
48. S. Schulz, C. Struck, *MNRAS* **328**, 185–202 (Nov. 2001).
49. V. Springel, *MNRAS* **364**, 1105–1134 (2005).
50. V. Springel, T. Di Matteo, L. Hernquist, *MNRAS* **361**, 776–794 (Aug. 2005).
51. V. Springel, S. D. M. White, G. Tormen, G. Kauffmann, *MNRAS* **328**, 726–750 (Dec. 2001).
52. V. Springel *et al.*, **435**, 629–636 (June 2005).
53. A. A. Starobinskii, *ZhETF Pisma Redaktsiiu* **30**, 719–723 (Dec. 1979).
54. L. J. Tacconi *et al.*, *ApJ* **853**, 179 (Feb. 2018).
55. The EAGLE team, *arXiv e-prints*, arXiv:1706.09899 (2017).
56. A. K. Upadhyay, K. A. Oman, S. C. Trager, *arXiv e-prints*, arXiv:2104.04388 (Apr. 2021).
57. F. van de Voort *et al.*, *MNRAS* **466**, 3460–3471 (Apr. 2017).
58. J. Wang *et al.*, *ApJ* **903**, 103 (Nov. 2020).
59. A. R. Wetzel, J. L. Tinker, C. Conroy, F. C. van den Bosch, *MNRAS* **432**, 336–358 (2013).
60. C. Wheeler, J. I. Phillips, M. C. Cooper, M. Boylan-Kolchin, J. S. Bullock, *MNRAS* **442**, 1396–1404 (Aug. 2014).
61. R. P. C. Wiersma, J. Schaye, B. D. Smith, *MNRAS* **393**, 99–107 (Feb. 2009).
62. R. P. C. Wiersma, J. Schaye, T. Theuns, C. Dalla Vecchia, L. Tornatore, *MNRAS* **399**, 574–600 (Oct. 2009).
63. R. J. Wright *et al.*, *MNRAS* **487**, 3740–3758 (Aug. 2019).
64. M.-Y. Zhuang, L. C. Ho, J. Shangguan, *ApJ* **906**, 38 (Jan. 2021).